This article has been accepted for publication in a future issue of this journal, but has not been fully edited. Content may change prior to final publication.
Citation information: DOI: 10.1109/TNNLS.2022.3209632, IEEE Transactions on Neural Networks and Learning Systems

Partial-Neurons-Based Proportional-Integral Observer Design for Artificial Neural Networks: A Multiple Description Encoding Scheme

Di Zhao, Zidong Wang, Yun Chen, Guoliang Wei, and Weiguo Sheng

***Abstract*—This paper is concerned with a new partial-neurons-based proportional-integral observer (PIO) design problem for a class of artificial neural networks subject to bounded disturbances. For the purpose of improving the reliability of the data transmission, the multiple description encoding mechanism is exploited to encode the measurement data into two identically important descriptions, and the encoded data are then transmitted to the decoders via two individual communication channels susceptible to packet dropouts, where Bernoulli-distributed stochastic variables are utilized to characterize the random occurrence of the packet dropouts. An explicit relationship is discovered that quantifies the influences from the packet dropouts on the decoding accuracy, and a sufficient condition is provided to assess the boundedness of the estimation error dynamics. Furthermore, the desired PIO parameters are calculated by solving two optimization problems based on two metrics (i.e. the smallest ultimate bound and the fastest decay rate) characterizing the estimation performance. Finally, the applicability and advantage of the proposed PIO design strategy are verified by means of an illustrative example.**

***Index Terms*—Artificial neural network, partial-neurons-based state estimation, proportional-integral observer, multiple description encoding scheme, packet dropout.**

I. Introduction

ARTIFICIAL neural network (ANN) is an information processing system that imitates the behavior characteristics of the human brain or animal nervous system. Owing to its outstanding performance in fault tolerance, parallelism, adaptability and self-organization, the ANN has found extensive applications in various fields including, but are not limited to, artificial intelligence, image recognition, signal processing [10], [12], [14], [16], [19], [33], [35], [37]. Therefore, the past few decades have seen an ever-growing enthusiasm towards the research on ANNs and, in particular, the dynamics analysis issues (e.g. stability, synchronization and state estimation problems) of ANNs have recently received considerable research interest, see e.g. [1], [26], [29], [40], [42], [48].

In the context of ANNs, the state information of the artificial neurons plays a crucially important role in accomplishing some specific tasks such as optimization, approximation and fault diagnosis. Unfortunately, the states of certain neurons might not be always acquirable for many reasons such as the large size of ANNs, the tight coupling between neurons, and the limits of network resources. In this case, an effective way is to estimate the state information of the neurons by making use of the available measurement outputs of the ANNs. Accordingly, much research effort has been devoted to the investigation of state estimation problems for ANNs, and some representative results can be found in [8], [21], [22], [25], [28], [38], [43].

A typical proportional-integral observer (PIO) contains both proportional and integral terms in its structure, and is therefore capable of simultaneously utilizing current and historical information. Compared to the traditional Luenberger observer that uses current information only, the PIO is in a better position to restrain steady-state error and enhance the insensitivity to parameter variations/noises, which are much desired in a great variety of engineering applications such as manufacturing, power system, network communication and aerospace [3], [4], [6], [45]. Accordingly, the PIO design problem has attracted a great deal of research interest [17], [18], [27], [31], [32] and some recent results concerning the PIO design specifically for ANNs can be found in [46], [47].

In practical engineering, it is quite common that certain neurons' measurements are inaccessible, and this leads to a substantial challenge in the state estimation of ANNs. Some typical causes for the partial unavailability of neuronal measurements include the large number of the neurons, the excessive complexity of the network topology, the scarcity of the network resources, as well as the harshness of the environment. In this case, one would have to estimate the neuron states by exploiting the accessible network measurements from a portion of the neurons only, and this gives rise to the so-called partial-neuron-based state estimation problem. Up to now, some preliminary results have been reported on the partial-neuron-based state estimation problems for ANNs [20], [24]. It is worth noting that the partial-neuron-based PIO design problem has not been thoroughly examined yet, and this constitutes the main motivation of our current study.

In the practical application of ANN, artificial neurons (and their connections) are often operated and monitored

This work was supported in part by the National Natural Science Foundation of China under Grants 62273239, 62103281, 61933007, 61973102, 61873148, 61873169 and 61873082, the Royal Society of the U.K., and the Alexander von Humboldt Foundation of Germany. (*Corresponding author: Guoliang Wei*.)

Di Zhao is with the College of Science, the Biomedical Engineering Postdoctoral Research Mobile Station, University of Shanghai for Science and Technology, Shanghai 200093, China. (Email: zhaodi0907520@163.com)

Zidong Wang is with the Department of Computer Science, Brunel University London, Uxbridge, Middlesex, UB8 3PH, United Kingdom. (Email: zidong.Wang@brunel.ac.uk)

Yun Chen is with the School of Automation, Hangzhou Dianzi University, Hangzhou 310018, China. (Email: yunchen@hdu.edu.cn)

Guoliang Wei is with the Business School, University of Shanghai for Science and Technology, Shanghai 200093, China. (Email: guoliang.wei@usst.edu.cn)

Weiguo Sheng is with the School of Information Science and Engineering, Hangzhou Normal University, Hangzhou 311121, China. (Email: weiguouk@hotmail.com)

This article has been accepted for publication in a future issue of this journal, but has not been fully edited. Content may change prior to final publication.
Citation information: DOI: 10.1109/TNNLS.2022.3209632, IEEE Transactions on Neural Networks and Learning Systems

in a remote way, where the corresponding information are transmitted via network-based communication mediums for the benefits of low cost and high reliability. Typically, an ANN has its measurements collected by the sensors and then transmitted to the remote estimator through the communication network, thereby facilitating the remote state monitoring. Network measurements are often massive high-throughput data and their transmission in the network medium (of limited communication capacity) is inevitably subject to channel congestion which, in turn, results in the phenomenon of data packet dropout. In this regard, it becomes a momentous task in ANN state estimation problems to leverage adequate data transmission mechanisms with a view of curbing data collisions and easing communication overheads. Accordingly, an increasing research interest has been paid to the state estimation problems for various ANNs under data transmission mechanisms, see e.g. [7], [34] and the references therein.

Among commonly deployed data transmission schemes in practice, the multiple description encoding scheme (MDES) has proven to be particularly efficient in mitigating the adverse impact induced by the packet dropout phenomenon and enhancing the reliability during data transmission. The MDES-based signal transmission consists of three steps, namely, 1) encoding the raw data into multiple descriptions with fewer bit occupancies and identical importance; 2) transmitting the descriptions to the decoder side via parallel independent channels; and 3) decoding the data to restore the original one by using the received descriptions. Note that more descriptions successfully transmitted to the decoder would lead to smaller decoding error and subsequently higher decoding accuracy.

Though MDES has been originated for the purpose of media communication, it has now been applied in a wide range of engineering systems such as distributed storage systems, diversity communication systems and image/audio/video encoding [2], [5], [9], [13], [15], [30], [39]. Nonetheless, despite its popularity in the general area of signal processing, the MDES has gained relatively little attention in the context of state estimation problems due primarily to the substantial challenge in appropriately handling the influence from decoding error on estimation performance, and this constitutes another motivation of our current investigation.

Concluding the literature review carried out so far, it makes both theoretical and practical sense to look into the partial-neurons-based PIO design problem for ANNs under the MDES. In doing so, we are confronted with three potential challenges outlined as follows. 1) For a given ANN with only partial accessible measurements, it appears non-trivial to modify the conventional PIO for the sake of estimating the states of all neurons. 2) With many kinds of data transmission strategies in hand, it is a demanding task to choose a proper one that not only alleviates the packet-dropout-induced impacts but also improves the reliability of data transmission. 3) In the presence of the decoding errors, it is mathematically difficult to pin down the boundedness condition of estimation error dynamics while quantifying the effects from the decoding errors on the estimation performance. It is, therefore, the main aim of this paper to cope with the above-identified challenges.

The primary contributions made in this paper are highlighted as follows: *1) a partial-neurons-based PIO is developed that is capable of estimating the all neuron states of ANNs by making use of the measurement information from a fraction of neurons only; 2) a MDES, which outperforms the traditional uniform-quantization-based encoding mechanism in error resilience, is implemented on the sensor-to-observer channel to elevate the reliability of the codeword transmission; and 3) sufficient conditions are established to assess the boundedness of the error dynamics of the partial-neurons-based state estimates and also reveal the joint influences from the randomly occurring packet dropout and decoding errors on the estimation performance.*

Notation. The notation used here is fairly standard except where otherwise stated. For a vector a, $\|a\|_2$ and $\|a\|_\infty$ describe the Euclidean norm and infinite norm, respectively. For $x, y \in \mathbb{N}^+$, let $\langle \frac{x}{y} \rangle$ be the remainder obtained on dividing x by y and let $\lfloor \frac{x}{y} \rfloor$ be the quotient, i.e. $x = y\lfloor \frac{x}{y} \rfloor + \langle \frac{x}{y} \rangle$.

II. Problem Formulation and Preliminaries

A. Model of The Artificial Neural Network

Consider an ANN with l neurons described by the following model:

$$x_\iota(k+1) = a_\iota x_\iota(k) + \sum_{\jmath=1}^{l} \omega_{\iota\jmath}\xi_\jmath\big(x_\jmath(k)\big) + b_\iota v_\iota(k) \quad (1)$$

for $\iota \in \mathfrak{L} \triangleq \{1, 2, \ldots, l\}$, where $x_\iota(k) \in \mathbb{R}$ is the state of the ιth neuron at time instant k; the scalars a_ι, b_ι and $\omega_{\iota\jmath}$ are known constants which represent the state feedback coefficient, the disturbance coefficient and the interconnection strength between neurons ι and $\jmath$, respectively; $v_\iota(k) \in \mathbb{R}$ denotes the disturbance input satisfying

$$\|v_\iota(k)\|^2 \leqslant \bar{v} \quad (2)$$

with $\bar{v} > 0$ being a given scalar. In addition, $\xi_\jmath(\cdot) : \mathbb{R} \to \mathbb{R}$ represents the activation function of the $\jmath$th neuron satisfying

$$\begin{aligned}\big(\xi_\jmath(p_1) - \xi_\jmath(p_2) - \acute{q}_\jmath(p_1 - p_2)\big)^T \\ \times \big(\xi_\jmath(p_1) - \xi_\jmath(p_2) - \grave{q}_\jmath(p_1 - p_2)\big) \leqslant 0\end{aligned} \quad (3)$$

and $\xi_\jmath(0) = 0$, for $\forall p_1, p_2 \in \mathbb{R}$, where $\acute{q}_\jmath$ and $\grave{q}_\jmath$ are known constants.

B. Measurements of Partial Neurons

As discussed previously, it is often the case in practice that only a fraction of neurons have their measurement outputs available for dynamics analysis. In this paper, without loss of generality, we assume that the outputs of the first h $(h < l)$ neurons can be accessed, which are modeled by

$$y_\imath(k) = c_\imath x_\imath(k) \quad (4)$$

where, for $\imath \in \mathfrak{H} \triangleq \{1, 2, \ldots, h\}$, $y_\imath(k) \in \mathbb{R}$ is the measurement output and $c_\imath$ is a known constant.

C. Multiple Description Encoding Scheme

In the realization of ANNs, data transmissions often suffers from the phenomenon of packet dropouts due to limited communication capacity. To improve the efficiency of resource utilization, the MDES is used to alleviate the adverse effects induced by the packet dropouts. As shown in Fig. 1, the two description encoding scheme is adopted in this paper. Under

This article has been accepted for publication in a future issue of this journal, but has not been fully edited. Content may change prior to final publication.
Citation information: DOI: 10.1109/TNNLS.2022.3209632, IEEE Transactions on Neural Networks and Learning Systems

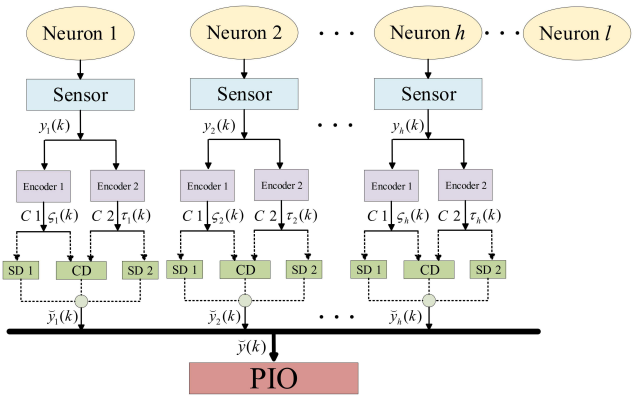

Fig. 1: Partial-neurons-based PIO design problem under MDES for ANN.

such a scheme, each sensor measurement is encoded into two different descriptions according to the corresponding encoding rules, and then the descriptions are simultaneously transmitted to the decoding devices via two mutually independent channels.

The mathematical model of the MDES can be expressed as follows.

Encoder:

$$\begin{cases} \varsigma_\imath(k) = \ell_\imath^r\big(y_\imath(k)\big) \\ \tau_\imath(k) = \ell_\imath^c\big(y_\imath(k)\big) \end{cases}, \quad (\imath \in \mathfrak{H}) \tag{5}$$

where $\ell_\imath^r(\cdot)$ and $\ell_\imath^c(\cdot)$ are two encoding functions, and $\varsigma_\imath(k)$ and $\tau_\imath(k)$ are two individual descriptions of $y_\imath(k)$.

Decoder:

$$\breve{y}_\imath(k) = \begin{cases} \hbar_\imath^u\big(\varsigma_\imath(k)\big), & \text{when } \phi^u(k)=1,\ \phi^d(k)=0 \\ \hbar_\imath^d\big(\tau_\imath(k)\big), & \text{when } \phi^u(k)=0,\ \phi^d(k)=1 \\ \hbar_\imath^c\big(\varsigma_\imath(k),\, \tau_\imath(k)\big), & \text{when } \phi^u(k)=1, \phi^d(k)=1 \\ \breve{y}_\imath(k-1), & \text{when } \phi^u(k)=0, \phi^d(k)=0 \end{cases} \tag{6}$$

where, for $\imath \in \mathfrak{H}$, $\breve{y}_\imath(k)$ is the decoding value corresponding to $y_\imath(k)$; $\hbar_\imath^u(\cdot)$ and $\hbar_\imath^d(\cdot)$ are two-side decoding functions and $\hbar_\imath^c(\cdot\,,\cdot)$ is the central decoding function. Here, two independent-identical-distribution Bernoulli sequences $\phi^u(k)$ and $\phi^d(k)$ are utilized to govern the phenomenon of packet dropout with probability distributions:

$$\begin{aligned} \text{Prob}\{\phi^u(k)=1\} &= \bar{\phi}_u, \quad \text{Prob}\{\phi^u(k)=0\} = 1-\bar{\phi}_u \\ \text{Prob}\{\phi^d(k)=1\} &= \bar{\phi}_d, \quad \text{Prob}\{\phi^d(k)=0\} = 1-\bar{\phi}_d. \end{aligned}$$

Remark 1: In accordance with (6) and Fig. 1, if no packet-dropout occurs (i.e. $\phi^u(k)=1$, $\phi^d(k)=1$), both the description packets $\varsigma_\imath(k)$ and $\tau_\imath(k)$ are received, and the central decoder $\hbar_\imath^c(\cdot\,,\cdot)$ (labeled as "CD") is enabled to perform the decoding operation. If the packet-dropout occurs in channel "C 1" only (i.e. $\phi^u(k)=0$, $\phi^d(k)=1$), only the description packet $\tau_\imath(k)$ is available to the side decoder $\hbar_\imath^d(\cdot)$ (labeled as "SD 2"). If the packet-dropout occurs in channel "C 2" only (i.e. $\phi^u(k)=1$, $\phi^d(k)=0$), only the description packet $\varsigma_\imath(k)$ is available and the side decoder $\hbar_\imath^u(\cdot)$ (labeled as "SD 1") is triggered to generate the decoded value. Furthermore, if the packet-dropout occurs in both channels "C 1" and "C 2" (i.e. $\phi^u(k)=0$, $\phi^d(k)=0$), neither of description packet is transmitted to the decoder. According to the zero-order holder (ZOH) strategy, the latest decoded measurement $\breve{y}_\imath(k-1)$ is utilized to generate the estimation signal.

Based on the above analysis, let us introduce three random variables $\zeta_n(k)$ $(n=0,\,1,\,2)$ as follows:

$$\zeta_n(k) \triangleq \delta\big(\phi(k),\, n\big), \quad \phi(k) \triangleq \phi^u(k) + \phi^d(k)$$

where $\sum_{n=0}^{2} \zeta_n(k) = 1$ and

$$\begin{aligned} \mathbb{E}\{\zeta_0(k)\} &\triangleq \bar{\zeta}_0 = (1-\bar{\phi}_u)(1-\bar{\phi}_d) \\ \mathbb{E}\{\zeta_1(k)\} &\triangleq \bar{\zeta}_1 = \bar{\phi}_u(1-\bar{\phi}_d) + \bar{\phi}_d(1-\bar{\phi}_u) \\ \mathbb{E}\{\zeta_2(k)\} &\triangleq \bar{\zeta}_2 = \bar{\phi}_u\bar{\phi}_d. \end{aligned}$$

Here, $\delta\{\cdot\,,\cdot\}$ is the Kronecker delta function defined as

$$\delta\{i\,,\,j\} = \begin{cases} 1, & i=j \\ 0, & i\neq j. \end{cases}$$

Denote the decoding error as $\varepsilon_{n,\,\imath}(k) \triangleq \breve{y}_\imath(k) - y_\imath(k)$ with n $(n=0,\,1,\,2)$ representing the number of received description packets. Abiding by the reception of the description packets at the decoder side and the ZOH strategy, the decoded measurement output $\breve{y}_\imath(k)$ is modeled as:

$$\begin{aligned} \breve{y}_\imath(k) =& \zeta_0(k)\breve{y}_\imath(k-1) + \zeta_1(k)\big(y_\imath(k) + \varepsilon_{1,\imath}(k)\big) \\ &+ \zeta_2(k)\big(y_\imath(k) + \varepsilon_{2,\imath}(k)\big) \\ =& \zeta_0(k)\breve{y}_\imath(k-1) + \big(1-\zeta_0(k)\big)y_\imath(k) \\ &+ \zeta_1(k)\varepsilon_{1,\imath}(k) + \zeta_2(k)\varepsilon_{2,\imath}(k). \end{aligned} \tag{7}$$

D. Partial-Neurons-Based PIO

By means of the decoded measurements from the first h neurons, the PIO to be designed is of the following form:

- for $\imath = 1,\, 2,\, \ldots,\, h$,

$$\begin{cases} \hat{x}_\imath(k+1) = a_\imath\hat{x}_\imath(k) + \displaystyle\sum_{\jmath=1}^{l} \omega_{\imath\jmath}\xi_\jmath\big(\hat{x}_\jmath(k)\big) \\ \qquad\qquad + f_{1,\imath}\varrho_\imath(k) + f_{2,\imath}\big(\breve{y}_\imath(k) - c_\imath\hat{x}_\imath(k)\big) \\ \varrho_\imath(k+1) = \varrho_\imath(k) + f_{3,\imath}\big(\breve{y}_\imath(k) - c_\imath\hat{x}_\imath(k)\big) \end{cases} \tag{8}$$

- for $\imath = h+1,\, h+2,\, \ldots,\, l$,

$$\hat{x}_\imath(k+1) = a_\imath\hat{x}_\imath(k) + \sum_{\jmath=1}^{l} \omega_{\imath\jmath}\xi_\jmath\big(\hat{x}_\jmath(k)\big) \tag{9}$$

where $\hat{x}_\imath(k) \in \mathbb{R}$ is the state estimate of the $\imath$th neuron; $\varrho(k) \in \mathbb{R}$ is the integral of the $\imath$th neuron's output estimation error; and $f_{1,\imath}$, $f_{2,\imath}$ and $f_{3,\imath}$ are the observer gains of the $\imath$th neuron.

Remark 2: In the practical application of ANNs, it is quite common that the outputs of some neurons are immeasurable/inaccessible because of the large network size and the complicated network topology. Accounting for this, a partial-neurons-based PIO is constructed, in which only the state estimates for the first h neurons are generated with "innovations". In fact, with more neurons having accessible measurement outputs, a better estimation performance can be achieved.

This article has been accepted for publication in a future issue of this journal, but has not been fully edited. Content may change prior to final publication.
Citation information: DOI: 10.1109/TNNLS.2022.3209632, IEEE Transactions on Neural Networks and Learning Systems

In the sequel, denoting $\tilde{x}_\iota(k) \triangleq x_\iota(k) - \hat{x}_\iota(k)$, the estimation error dynamics for ιth neuron is obtained as:

- for $\iota = 1, 2, \ldots, h$,

$$\begin{cases} \tilde{x}_\iota(k+1) = (a_\iota - f_{2,\iota}c_\iota)\tilde{x}_\iota(k) + b_\iota v_\iota(k) + \sum_{\jmath=1}^{l}\omega_{\iota\jmath}\tilde{\xi}_\jmath(k) \\ \qquad\qquad - f_{1,\iota}\varrho_\iota(k) - \zeta_0(k)f_{2,\iota}\varepsilon_{0,\iota}(k) \\ \qquad\qquad - \zeta_1(k)f_{2,\iota}\varepsilon_{1,\iota}(k) - \zeta_2(k)f_{2,\iota}\varepsilon_{2,\iota}(k) \\ \varrho_\iota(k+1) = \varrho_\iota(k) + f_{3,\iota}c_\iota\tilde{x}_\iota(k) + \zeta_0(k)f_{3,\iota}\varepsilon_{0,\iota}(k) \\ \qquad\qquad + \zeta_1(k)f_{3,\iota}\varepsilon_{1,\iota}(k) + \zeta_2(k)f_{3,\iota}\varepsilon_{2,\iota}(k) \end{cases} \tag{10}$$

- for $\iota = h+1, h+2, \ldots, l$,

$$\tilde{x}_\iota(k+1) = a_\iota\tilde{x}_\iota(k) + b_\iota v_\iota(k) + \sum_{\jmath=1}^{l}\omega_{\iota\jmath}\tilde{\xi}_\jmath(k) \tag{11}$$

where

$$\tilde{\xi}_\iota(k) \triangleq \xi\big(x_\iota(k)\big) - \xi\big(\hat{x}_\iota(k)\big).$$

For presentation clarity, we introduce the following notations:

$$\begin{aligned} \varepsilon_0(k) &\triangleq \begin{bmatrix}\varepsilon_{0,1}(k) & \varepsilon_{0,2}(k) & \cdots & \varepsilon_{0,h}(k)\end{bmatrix}^T \\ \varepsilon_1(k) &\triangleq \begin{bmatrix}\varepsilon_{1,1}(k) & \varepsilon_{1,2}(k) & \cdots & \varepsilon_{1,h}(k)\end{bmatrix}^T \\ \varepsilon_2(k) &\triangleq \begin{bmatrix}\varepsilon_{2,1}(k) & \varepsilon_{2,2}(k) & \cdots & \varepsilon_{2,h}(k)\end{bmatrix}^T \\ \tilde{x}(k) &\triangleq \begin{bmatrix}\tilde{x}_1(k) & \tilde{x}_2(k) & \cdots & \tilde{x}_l(k)\end{bmatrix}^T \\ \tilde{\xi}(k) &\triangleq \begin{bmatrix}\tilde{\xi}_1(k) & \tilde{\xi}_2(k) & \cdots & \tilde{\xi}_l(k)\end{bmatrix}^T \\ v(k) &\triangleq \begin{bmatrix}v_1(k) & v_2(k) & \cdots & v_l(k)\end{bmatrix}^T \\ y(k) &\triangleq \begin{bmatrix}y_1(k) & y_2(k) & \cdots & y_h(k)\end{bmatrix}^T \\ \breve{y}(k) &\triangleq \begin{bmatrix}\breve{y}_1(k) & \breve{y}_2(k) & \cdots & \breve{y}_h(k)\end{bmatrix}^T \\ \varrho(k) &\triangleq \begin{bmatrix}\varrho_1(k) & \varrho_2(k) & \cdots & \varrho_h(k)\end{bmatrix}^T \\ A &= \text{diag}\{a_1, \quad a_2, \quad \ldots, \quad a_l\} \\ B &= \text{diag}\{b_1, \quad b_2, \quad \ldots, \quad b_l\} \\ C_0 &= \text{diag}\{c_1, \quad c_2, \quad \ldots, \quad c_h\} \\ F_{0,1} &= \text{diag}\{f_{1,1}, \quad f_{1,2}, \quad \ldots, \quad f_{1,h}\} \\ F_{0,2} &= \text{diag}\{f_{2,1}, \quad f_{2,2}, \quad \ldots, \quad f_{2,h}\} \\ F_3 &= \text{diag}\{f_{3,1}, \quad f_{3,2}, \quad \ldots, \quad f_{3,h}\} \\ C &= \begin{bmatrix}C_0 & \mathbf{0}_{h\times(l-h)}\end{bmatrix}, \quad W = [\omega_{\iota\jmath}]_{l\times l} \\ F_1 &= \begin{bmatrix}F_{0,1} \\ \mathbf{0}_{(l-h)\times h}\end{bmatrix}, \; F_2 = \begin{bmatrix}F_{0,2} \\ \mathbf{0}_{(l-h)\times h}\end{bmatrix}. \end{aligned}$$

Accordingly, the estimation error dynamics can be rearranged in the following compact form:

$$\begin{cases} \tilde{x}(k+1) = (A - F_2C)\tilde{x}(k) + Bv(k) + W\tilde{\xi}(k) \\ \qquad\qquad - F_1\varrho(k) - \zeta_0(k)F_2\varepsilon_0(k) \\ \qquad\qquad - \zeta_1(k)F_2\varepsilon_1(k) - \zeta_2(k)F_2\varepsilon_2(k) \\ \varrho(k+1) = \varrho(k) + F_3C\tilde{x}(k) + \zeta_0(k)F_3\varepsilon_0(k) \\ \qquad\qquad + \zeta_1(k)F_3\varepsilon_1(k) + \zeta_2(k)F_3\varepsilon_2(k). \end{cases} \tag{12}$$

By setting $\vartheta(k) \triangleq \begin{bmatrix}\tilde{x}^T(k) & \varrho^T(k)\end{bmatrix}^T$, one obtains the following augmented system:

$$\begin{aligned} \vartheta(k+1) = &\mathscr{A}\vartheta(k) + \mathscr{W}\tilde{\xi}(k) + \mathscr{B}v(k) \\ &+ \big(\check{\zeta}_0(k) + \bar{\zeta}_0\big)\mathscr{F}\varepsilon_0(k) \\ &+ \big(\check{\zeta}_1(k) + \bar{\zeta}_1\big)\mathscr{F}\varepsilon_1(k) \\ &+ \big(\check{\zeta}_2(k) + \bar{\zeta}_2\big)\mathscr{F}\varepsilon_2(k) \end{aligned} \tag{13}$$

where

$$\begin{aligned} \mathscr{A} &\triangleq \begin{bmatrix}A - F_2C & -F_1 \\ F_3C & I\end{bmatrix}, \; \mathscr{W} \triangleq \begin{bmatrix}W \\ \mathbf{0}\end{bmatrix}, \; \mathscr{B} \triangleq \begin{bmatrix}B \\ \mathbf{0}\end{bmatrix} \\ \mathscr{F} &\triangleq \begin{bmatrix}-F_2 \\ F_3\end{bmatrix}, \quad \check{\zeta}_0(k) \triangleq \zeta_0(k) - \bar{\zeta}_0 \\ \check{\zeta}_1(k) &\triangleq \zeta_1(k) - \bar{\zeta}_1, \quad \check{\zeta}_2(k) \triangleq \zeta_2(k) - \bar{\zeta}_2. \end{aligned}$$

E. Problem Statement

Definition 1: The dynamics of the augmented system (13) is said to be exponentially ultimately bounded in mean-square sense if there exist constants $0 < \alpha < 1$, $\beta > 0$ and $\gamma > 0$ such that

$$\mathbb{E}\{\|\vartheta(k)\|^2\} \leqslant \alpha^k\beta + \gamma, \quad \forall k \geqslant 0 \tag{14}$$

where γ is said to be an asymptotic upper bound of $\|\vartheta(k)\|^2$ in mean-square sense.

The objective of this paper is to devise a PIO for ANN (1) by using decoded measurements from only a part of neurons such that a) the exponentially mean-square ultimate boundedness of the augmented system (13) is guaranteed subject to bounded disturbance $v(k)$ and the decoding errors $\varepsilon_0(k)$, $\varepsilon_1(k)$, $\varepsilon_2(k)$, and b) appropriate observer parameters are determined through minimizing the attained upper bounds or maximizing the decay rate.

III. Main Results

A. Multiple Description Encoding Procedure

In this subsection, we endeavor to formalize the encoding procedure through two steps, namely, *the index generation step* and *the index assignment step*. Specifically, the measurement output is quantified into the corresponding index by the index generation operation, and then the generated index is assigned to the corresponding cell of a certain mapping matrix on the basis of the nested index assignment principle [36].

Index Generation: To begin with, the scalar quantizer $\eta_h(\cdot) : \mathbb{R} \to \mathbb{R}$ is constructed as follows:

$$\eta_h(z) = \begin{cases} d, & z \geqslant d \\ -d, & z \leqslant -d \\ -d + \dfrac{(2t-1)d}{g}, & -d + u_1 \leqslant z \leqslant -d + u_2 \end{cases} \tag{15}$$

where $z \in \mathbb{R}$ denotes the signal to be processed; d is a known scalar representing the saturation value; g is a positive integer corresponding to the quantization level; u_1 and u_2 are defined by $u_1 \triangleq 2(t-1)dg^{-1}$ and $u_2 \triangleq 2tdg^{-1}$, respectively, for $t \in \mathfrak{G} \triangleq \{1, 2, \ldots, g\}$. As can be seen from (15), the interval $[-d, d]$ is divided into g parts $\Re_i(d)$ $(i \in \mathfrak{G})$ with

$$\Re_i(d) = \big[-d + 2(i-1)dg^{-1}, \; -d + 2idg^{-1}\big)$$

and

$$\Re_i(d) \bigcap \Re_j(d) = \emptyset$$

This article has been accepted for publication in a future issue of this journal, but has not been fully edited. Content may change prior to final publication.
Citation information: DOI: 10.1109/TNNLS.2022.3209632, IEEE Transactions on Neural Networks and Learning Systems

for any $(i, j \in \mathfrak{G})$ and $i \neq j$.

To ensure that the quantizer $\eta_\imath(\cdot)$ is not saturated, we introduce an adjustable parameter $\pi_\imath$ and define

$$\eta_\imath\big(y_\imath(k)\big) \triangleq \pi_\imath \eta_\imath\big(\frac{y_\imath(k)}{\pi_\imath}\big)$$

such that, once $|y_\imath(k)| > d$, $y_\imath(k)/\pi_\imath$ belongs to the interval $[-d,\, d]$. Consequently, it can be concluded that the quantization error $\epsilon_\imath(k) \triangleq y_\imath(k) - \eta_\imath\big(y_\imath(k)\big)$ is computed as

$$|\epsilon_\imath(k)| \leqslant \frac{\pi_\imath d}{g}. \tag{16}$$

For $\eta_\imath\big(y_\imath(k)\big) \in \Re_{m_\imath(k)}(d)$, the following index is generated

$$\theta_\imath\Big(\eta_\imath\big(y_\imath(k)\big)\Big) = m_\imath(k) \tag{17}$$

with $m_\imath(k) \in \mathfrak{G}$ and $\imath \in \mathfrak{H}$.

Index Assignment: The generated index $m_\imath(k)$ can be assigned into the corresponding cell of the mapping matrix $\mathcal{M}$ by applying the nested assignment principle. Without loss of generality, we assume that the mapping matrix $\mathcal{M}$ is a $p \times p$ matrix with p being an even number. Subsequently, in the light of the location in the mapping matrix $\mathcal{M}$, a pair of descriptions $\big(\varsigma_\imath(k), \tau_\imath(k)\big)$ is determined. Here, $\varsigma_\imath(k)$ and $\tau_\imath(k)$ correspond to the row and column locations, respectively.

The index assignment function $\chi_\imath(\cdot):\ \mathbb{N}^+ \to \mathbb{N}^+ \times \mathbb{N}^+$ is given as

$$\begin{aligned}
&\chi_\imath\big(m_\imath(k)\big) \triangleq \Big(\chi_\imath^r\big(m_\imath(k)\big),\, \chi_\imath^c\big(m_\imath(k)\big)\Big) \\
&= \begin{cases}
\big(\mu_\imath(k)+1,\, \mu_\imath(k)+1\big), & \text{if } \nu_\imath(k) = 1 \\
\big(\mu_\imath(k)+1,\, \mu_\imath(k)\big), & \text{if } \nu_\imath(k) = 0 \text{ and } \mu_\imath(k) \text{ is even} \\
\big(\mu_\imath(k),\, \mu_\imath(k)+1\big), & \text{if } \nu_\imath(k) = 0 \text{ and } \mu_\imath(k) \text{ is odd} \\
\big(\mu_\imath(k)+2,\, \mu_\imath(k)+1\big), & \text{if } \nu_\imath(k) = 2 \text{ and } \mu_\imath(k) \text{ is even} \\
\big(\mu_\imath(k)+1,\, \mu_\imath(k)+2\big), & \text{if } \nu_\imath(k) = 2 \text{ and } \mu_\imath(k) \text{ is odd}
\end{cases}
\end{aligned} \tag{18}$$

with

$$\begin{aligned}
\mu_\imath(k) &= \lfloor \frac{m_\imath(k)}{2q+1} \rfloor = \lfloor \frac{m_\imath(k)}{3} \rfloor \\
\nu_\imath(k) &= \langle \frac{m_\imath(k)}{2q+1} \rangle = \langle \frac{m_\imath(k)}{3} \rangle.
\end{aligned}$$

Here, $\chi_i^r(\cdot)$ denotes the row assignment function and $\chi_i^c(\cdot)$ stands for the column assignment function, by which the single description $m_\imath(k)$ is mapped into the description pair $\big(\varsigma_\imath(k),\, \tau_\imath(k)\big)$ with

$$\begin{cases}
\varsigma_\imath(k) = \chi_i^r\big(m_\imath(k)\big) \\
\tau_\imath(k) = \chi_i^c\big(m_\imath(k)\big).
\end{cases}$$

In this case, the encoding functions $\ell_i^r(\cdot)$ and $\ell_i^c(\cdot)$ in (5) are presented as follows:

$$\begin{cases}
\ell_i^r\big(y_\imath(k)\big) = \chi_i^r\Big(\theta_\imath\Big(\eta_\imath\big(y_\imath(k)\big)\Big)\Big) \\
\ell_i^c\big(y_\imath(k)\big) = \chi_i^c\Big(\theta_\imath\Big(\eta_\imath\big(y_\imath(k)\big)\Big)\Big).
\end{cases} \tag{19}$$

Remark 3: According to the regulations of the nested assignment principle stated in [36], the cells located on the main diagonal and the nearest $2q$ diagonal of the mapping matrix are used to place the corresponding indices. In this paper, we are interested in the mapping matrix only for the case $q = 1$. In this sense, the cells located on the main diagonal and its nearest 2 diagonals of the mapping matrix are placed indices, and the example of the nested assignment principle with $p = 8$ and $q = 1$ is showcased in Fig. 2.

1	3						
2	4	5					
	6	7	9				
		8	10	11			
			12	13	15		
				14	16	17	
					18	19	21
						20	22

Fig. 2: Nested index assignment for $p = 8$ and $q = 1$ in [36].

B. Decoding Procedure

In this subsection, we are interested in developing a decoder by using the received codewords. The key point of the decoding procedure is to obtain the decoded value $\breve{y}_\imath(k)$ as accurately as possible based on the received location information of the index $m_\imath(k)$ in the mapping matrix $\mathcal{M}$. Note that, owing to the possible dropout of the description packets $\varsigma_\imath(k)$ (the row number) and $\tau_\imath(k)$ (the column number) during data transmission, the value of index $m_\imath(k)$ might be inaccurate and thus the decoding accuracy might be unqualified. In view of this, one viable way to achieve the desired decoding accuracy is to construct an index estimator for the sake of obtaining an estimate of the index $m_\imath(k)$ in terms of the reception of the descriptions.

The following index estimation strategies are developed based on the individual situation of the available descriptions at the decoder side.

- **Case 1:** neither of channels suffers from the packet dropouts. The central decoder is activated to determine the estimated index $\hat{m}_\imath(k)$ based on the available descriptions $\varsigma_\imath(k)$ and $\tau_\imath(k)$. The estimated index $\hat{m}_\imath(k)$ can be explicitly calculated as follows:

$$\begin{aligned}
&\hat{m}_\imath(k) \triangleq \sigma_i^c\big(\varsigma_\imath(k),\, \tau_\imath(k)\big) \\
&= \begin{cases}
3\varsigma_\imath(k) - 2, & \text{if } \varsigma_\imath(k) = \tau_\imath(k) \\
3\varsigma_\imath(k) - 3, & \text{if } \varsigma_\imath(k) = \tau_\imath(k) + 1 \text{ and } \varsigma_\imath(k) \text{ is odd} \\
3\varsigma_\imath(k), & \text{if } \varsigma_\imath(k) = \tau_\imath(k) - 1 \text{ and } \varsigma_\imath(k) \text{ is odd} \\
3\varsigma_\imath(k) - 4, & \text{if } \varsigma_\imath(k) = \tau_\imath(k) + 1 \text{ and } \varsigma_\imath(k) \text{ is even} \\
3\varsigma_\imath(k) - 1, & \text{if } \varsigma_\imath(k) = \tau_\imath(k) - 1 \text{ and } \varsigma_\imath(k) \text{ is even}
\end{cases}
\end{aligned} \tag{20}$$

  where $\sigma_i^c(\cdot,\, \cdot)$ is the index estimation function. It is not difficult to find that the estimation accuracy is 100% and the index estimation error is

$$\tilde{m}_\imath(k) \triangleq \hat{m}_\imath(k) - m_\imath(k) = 0 \tag{21}$$

- **Case 2:** only one of the channels suffers from the packet dropouts. If the packet-dropout occurs in channel "C 1",

This article has been accepted for publication in a future issue of this journal, but has not been fully edited. Content may change prior to final publication. Citation information: DOI: 10.1109/TNNLS.2022.3209632, IEEE Transactions on Neural Networks and Learning Systems

decoder "SD 2" is triggered to determine the estimated index $\hat{m}_\imath(k)$ based on the received description $\tau_\imath(k)$. In this case, we set the diagonal element of the $\tau_\imath(k)$-th column as the estimation of $m_\imath(k)$, which is determined as

$$\hat{m}_\imath(k) \triangleq \sigma_\imath^d\big(\tau_\imath(k)\big) = 3\tau_\imath(k) - 2. \tag{22}$$

If the packet-dropout occurs in channel "C 2", decoder "SD 1" is enabled to determine the estimated index $\hat{m}_\imath(k)$ based on the received description $\varsigma_\imath(k)$. Similarly, the diagonal element of the $\varsigma_\imath(k)$-th row is utilize to generate the estimation of $m_\imath(k)$. Accordingly, we have

$$\hat{m}_\imath(k) \triangleq \sigma_\imath^u\big(\varsigma_\imath(k)\big) = 3\varsigma_\imath(k) - 2. \tag{23}$$

Here, $\sigma_\imath^d(\cdot)$ and $\sigma_\imath^u(\cdot)$ are the index estimation functions. From (22)-(23), we can easily find that

$$|\tilde{m}_\imath(k)| \leqslant 2. \tag{24}$$

- **Case 3:** both of channels "C 1" and "C 2" suffer from the packet dropouts. In such a case, based on the ZOH strategy, the latest decoded measurement $\breve{y}_\imath(k-1)$ is directly employed to compensate the value of $\breve{y}_\imath(k)$.

C. Analysis of the Decoding Error

After developing the encoding and decoding procedures, we are now in a position to conduct a detailed mathematical analysis for the purpose of evaluating the decoding error in a quantitative way.

Theorem 1: For the MDES (5)-(6), the decoding error between the measurement $y_\imath(k)$ and the decoded value $\breve{y}_\imath(k)$ ($\imath \in \mathfrak{H}$) satisfies

$$\varepsilon_\imath(k) = \begin{cases} \varepsilon_{1,\imath}(k), & \text{for the side decoder} \\ \varepsilon_{2,\imath}(k), & \text{for the central decoder} \end{cases} \tag{25}$$

and

$$\begin{cases} |\varepsilon_{1,\imath}(k)| \leqslant 5\epsilon_\imath(k) \\ |\varepsilon_{2,\imath}(k)| \leqslant \epsilon_\imath(k) \end{cases}. \tag{26}$$

Proof: To begin with, by recurring to the expressions of $\mu_\imath(k)$ and $\nu_\imath(k)$, we have

$$m_\imath(k) = 3\mu_\imath(k) + \nu_\imath(k). \tag{27}$$

In line with (18) and (22)-(23), the index estimation error satisfies

$$|\tilde{m}_\imath(k)| \leqslant \begin{cases} 0, & \text{two descriptions are received} \\ 2, & \text{one description is received} \end{cases} \tag{28}$$

Based on (20) and (22)-(23), the inverse quantization function can be constructed as follows:

$$\hat{\eta}_\hbar\big(\hat{m}_\imath(k)\big) \triangleq -d + \frac{\big(2\hat{m}_\imath(k) - 1\big)d}{g} \tag{29}$$

for $\hat{m}_\imath(k) \in \mathfrak{G}$. Consequently, the decoder functions can be expressed as

$$\begin{cases} \hbar_\imath^u\big(\varsigma_\imath(k)\big) = \hat{\eta}_\hbar\Big(\sigma_\imath^u\big(\varsigma_\imath(k)\big)\Big) \\ \hbar_\imath^d\big(\tau_\imath(k)\big) = \hat{\eta}_\hbar\Big(\sigma_\imath^d\big(\tau_\imath(k)\big)\Big) \\ \hbar_\imath^c\big(\varsigma_\imath(k),\, \tau_\imath(k)\big) = \hat{\eta}_\hbar\Big(\sigma_\imath^c\big(\varsigma_\imath(k),\, \tau_\imath(k)\big)\Big). \end{cases} \tag{30}$$

Bearing (30) in mind, we have the conclusion that the decoding error $\varepsilon_\imath(k)$ satisfies (25)-(26), which ends the proof. ■

Remark 4: Inspired by (25)-(26), we can rewrite the decoding error as follows

$$\begin{aligned} \varepsilon(k) =& \zeta_0(k)\|\varepsilon_0(k)\| + \zeta_1(k)\|\varepsilon_1(k)\| \\ &+ \zeta_2(k)\|\varepsilon_2(k)\|. \end{aligned} \tag{31}$$

Combining (25)-(26) together yields

$$\|\varepsilon_1(k)\| \leqslant \varpi_1(k) \triangleq \sqrt{\sum_{\imath=1}^{h}\big(5\epsilon_\imath(k)\big)^2} \tag{32}$$

and

$$\|\varepsilon_2(k)\| \leqslant \varpi_2(k) \triangleq \sqrt{\sum_{\imath=1}^{h}\big(\epsilon_\imath(k)\big)^2}. \tag{33}$$

Furthermore, when neither of the description packets is transmitted to the decoder, a reasonable assumption is that the upper bound of $\|\varepsilon_0(k)\|$ is greater than $\varpi_1(k)$. Recalling the condition $\varpi_1(k) = 5\varpi_2(k)$, there exists a positive scalar $\kappa > 5$ such that

$$\|\varepsilon_0(k)\| \leqslant \kappa\varpi_2(k). \tag{34}$$

Defining $\bar{\varepsilon}(k) \triangleq \mathbb{E}\{\varepsilon(k)\}$ as the average decoding error, we obtain

$$\begin{aligned} \bar{\varepsilon}(k) =& \mathbb{E}\{\zeta_0(k)\}\|\varepsilon_0(k)\| + \mathbb{E}\{\zeta_1(k)\}\|\varepsilon_1(k)\| \\ &+ \mathbb{E}\{\zeta_2(k)\}\|\varepsilon_2(k)\| \\ =& \bar{\zeta}_0\|\varepsilon_0(k)\| + \bar{\zeta}_1\|\varepsilon_1(k)\| + \bar{\zeta}_2\|\varepsilon_2(k)\| \\ \leqslant& \bar{\zeta}_0\kappa\varpi_2(k) + \bar{\zeta}_1\varpi_1(k) + \bar{\zeta}_2\varpi_2(k) \\ =& (\kappa\bar{\zeta}_0 + 5\bar{\zeta}_1 + \bar{\zeta}_2)\varpi_2(k) \\ \triangleq& \aleph\big(\bar{\phi}_u, \bar{\phi}_d, \varpi_2(k)\big). \end{aligned} \tag{35}$$

It is easy to see that $\aleph\big(\bar{\phi}_u, \bar{\phi}_d, \varpi_2(k)\big)$ is monotonically decreasing with respect to $\bar{\phi}_u$ and $\bar{\phi}_d$. As such, we draw the conclusion that, with the decrease of packet dropout rate (i.e. the increase of $\bar{\phi}_u$ or $\bar{\phi}_d$), the upper bound of the average decoding error would decrease as well, which caters to the practical engineering.

D. Analysis of the Estimation Error

To start with, a useful lemma is provided as follows to facilitate the subsequent derivation.

Lemma 1: For any real-valued vectors $\hat{z}$, $\check{z}$, and matrix $Y > 0$ of compatible dimensions, the following holds:

$$\hat{z}^T Y \check{z} + \check{z}^T Y \hat{z} \leqslant \varphi\hat{z}^T Y \hat{z} + \frac{1}{\varphi}\check{z}^T Y \check{z} \tag{36}$$

where $\varphi > 0$ is a given constant.

Theorem 2: Let the positive scalars φ_1, φ_2, φ_3, φ_4, φ_5, φ_6, the observer gain matrices F_1, F_2 and F_3 be given. Suppose that there exist positive scalars ψ_1, ψ_2, ψ_3, ψ_4, ψ_5, ψ_6, and positive definite matrix Z satisfying the following inequality:

$$\Psi_1 = \begin{bmatrix} \Psi_1^1 & \star \\ \Psi_1^2 & \Psi_1^3 \end{bmatrix} < 0 \tag{37}$$

This article has been accepted for publication in a future issue of this journal, but has not been fully edited. Content may change prior to final publication.
Citation information: DOI: 10.1109/TNNLS.2022.3209632, IEEE Transactions on Neural Networks and Learning Systems

where

$$\Psi_1^1 \triangleq \text{diag}\{\Psi_1^4,\ -\psi_2 I,\ -\psi_3 I,\ -\psi_4 I,\ -\psi_5 I,\}$$

$$\Psi_1^2 \triangleq \begin{bmatrix} \mathscr{A} & \mathscr{W} & \mathscr{B} & \bar{\zeta}_0\mathscr{F} & \mathbf{0} & \mathbf{0} \\ \Psi_1^5 & \mathbf{0} & \mathbf{0} & \mathbf{0} & \mathbf{0} & \mathbf{0} \\ \mathbf{0} & \Psi_1^6 & \mathbf{0} & \mathbf{0} & \mathbf{0} & \mathbf{0} \\ \mathbf{0} & \mathbf{0} & \Psi_1^7 & \mathbf{0} & \mathbf{0} & \mathbf{0} \\ \mathbf{0} & \mathbf{0} & \mathbf{0} & \mathbf{0} & \Psi_1^8 & \mathbf{0} \\ \mathbf{0} & \mathbf{0} & \mathbf{0} & \mathbf{0} & \mathbf{0} & \Psi_1^9 \end{bmatrix}$$

$$\Psi_1^3 \triangleq -I_6 \otimes Z^{-1},\ \Psi_1^4 \triangleq \begin{bmatrix} -Z + \psi_1 Z - \psi_6 \bar{Q}_1 & \star \\ \psi_6 \bar{Q}_2 & -\psi_6 I \end{bmatrix}$$

$$\Psi_1^5 \triangleq \sqrt{\varphi_1 + \varphi_4}\mathscr{A}, \quad \Psi_1^6 \triangleq \sqrt{\varphi_2 + \varphi_5}\mathscr{W}$$

$$\Psi_1^7 \triangleq \sqrt{\varphi_3 + \varphi_6}\mathscr{B}, \quad \Psi_1^8 \triangleq \sqrt{\bar{\zeta}_1 + \frac{\bar{\zeta}_1^2}{\varphi_1} + \frac{\bar{\zeta}_1^2}{\varphi_2} + \frac{\bar{\zeta}_1^2}{\varphi_3}}\mathscr{F}$$

$$\Psi_1^9 \triangleq \sqrt{\bar{\zeta}_2 + \frac{\bar{\zeta}_2^2}{\varphi_4} + \frac{\bar{\zeta}_2^2}{\varphi_5} + \frac{\bar{\zeta}_2^2}{\varphi_6}}\mathscr{F}, \quad \bar{Q}_1 \triangleq \text{diag}\{Q_1, 0\}$$

$$\bar{Q}_2 \triangleq \begin{bmatrix} Q_2 & 0 \end{bmatrix}, \quad q_{1,\jmath} \triangleq \acute{q}_\jmath \grave{q}_\jmath, \quad q_{2,\jmath} \triangleq \frac{\acute{q}_\jmath + \grave{q}_\jmath}{2}\ (\jmath \in \mathfrak{L})$$

$$Q_1 \triangleq \text{diag}\{q_{1,1}, \quad q_{1,2}, \quad \ldots, \quad q_{1,l}\}$$

$$Q_2 \triangleq \text{diag}\{q_{2,1}, \quad q_{2,2}, \quad \ldots, \quad q_{2,l}\}.$$

Then, the dynamics of the augmented system (13) is exponentially ultimately bounded in mean-square sense and the asymptotic upper bound is given by

$$\gamma = \frac{\psi_2\bar{v} + (\kappa\psi_3 + \kappa\bar{\zeta}_0 + 5\psi_4 + \psi_5)\sqrt{\sum_{\imath=1}^{h}\left(\frac{\pi_\imath d}{g}\right)^2}}{\lambda_{\min}(Z)\psi_1}. \tag{38}$$

Proof: Construct the following Lyapunov functional candidate:

$$V\big(\vartheta(k)\big) = \vartheta^T(k) Z \vartheta(k). \tag{39}$$

Accordingly, the difference of $V\big(\vartheta(k)\big)$ is expressed as

$$\Re V\big(\vartheta(k)\big) = \mathbb{E}\{V\big(\vartheta(k+1)\big)|\vartheta(k)\} - V\big(\vartheta(k)\big) \tag{40}$$

and then we have

$$\begin{aligned}
&\mathbb{E}\left\{\Re V\big(\vartheta(k)\big)\right\} \\
=&\mathbb{E}\left\{V\big(\vartheta(k+1)\big) - V\big(\vartheta(k)\big)\right\} \\
=&\mathbb{E}\Big\{\Big(\mathscr{A}\vartheta(k) + \mathscr{W}\tilde{\xi}(k) + \mathscr{B}v(k) + \big(\check{\zeta}_0(k) + \bar{\zeta}_0\big)\mathscr{F} \\
&\times \varepsilon_0(k) + \big(\check{\zeta}_1(k) + \bar{\zeta}_1\big)\mathscr{F}\varepsilon_1(k) + \big(\check{\zeta}_2(k) + \bar{\zeta}_2\big)\mathscr{F} \\
&\times \varepsilon_2(k)\Big)^T Z\Big(\mathscr{A}\vartheta(k) + \mathscr{W}\tilde{\xi}(k) + \mathscr{B}v(k) \\
&+ \big(\check{\zeta}_0(k) + \bar{\zeta}_0\big)\mathscr{F}\varepsilon_0(k) + \big(\check{\zeta}_1(k) + \bar{\zeta}_1\big)\mathscr{F}\varepsilon_1(k) \\
&+ \big(\check{\zeta}_2(k) + \bar{\zeta}_2\big)\mathscr{F}\varepsilon_2(k)\Big) - \vartheta^T(k) Z \vartheta(k)\Big\} \\
=&\mathbb{E}\Big\{\vartheta^T(k)\big(\mathscr{A}^T Z \mathscr{A} - Z\big)\vartheta(k) + \tilde{\xi}^T(k)\mathscr{W}^T Z \mathscr{W}\tilde{\xi}(k) \\
&+ v^T(k)\mathscr{B}^T Z \mathscr{B} v(k) + \big(\check{\zeta}_0(k) + \bar{\zeta}_0\big)^2 \varepsilon_0^T(k)\mathscr{F}^T \\
&\times Z\mathscr{F}\varepsilon_0(k) + \big(\check{\zeta}_1(k) + \bar{\zeta}_1\big)^2 \varepsilon_1^T(k)\mathscr{F}^T Z\mathscr{F}\varepsilon_1(k) \\
&+ \big(\check{\zeta}_2(k) + \bar{\zeta}_2\big)^2 \varepsilon_2^T(k)\mathscr{F}^T Z\mathscr{F}\varepsilon_2(k) + 2\tilde{\xi}^T(k)\mathscr{W}^T \\
&\times Z\mathscr{A}\vartheta(k) + 2v^T(k)\mathscr{B}^T Z\mathscr{A}\vartheta(k) + 2v^T(k)\mathscr{B}^T \\
&\times Z\mathscr{W}\tilde{\xi}(k) + 2\big(\check{\zeta}_0(k) + \bar{\zeta}_0\big)\varepsilon_0^T(k)\mathscr{F}^T Z\mathscr{A}\vartheta(k) \\
&+ 2\big(\check{\zeta}_0(k) + \bar{\zeta}_0\big)\varepsilon_0^T(k)\mathscr{F}^T Z\mathscr{W}\tilde{\xi}(k) + 2\big(\check{\zeta}_0(k) + \bar{\zeta}_0\big) \\
&\times \varepsilon_0^T(k)\mathscr{F}^T Z\mathscr{B}v(k) + 2\big(\check{\zeta}_1(k) + \bar{\zeta}_1\big)\varepsilon_1^T(k)\mathscr{F}^T Z \\
&\times \mathscr{A}\vartheta(k) + 2\big(\check{\zeta}_1(k) + \bar{\zeta}_1\big)\varepsilon_1^T(k)\mathscr{F}^T Z\mathscr{W}\tilde{\xi}(k) \\
&+ 2\big(\check{\zeta}_1(k) + \bar{\zeta}_1\big)\varepsilon_1^T(k)\mathscr{F}^T Z\mathscr{B}v(k) + 2\big(\check{\zeta}_0(k) + \bar{\zeta}_0\big) \\
&\times \big(\check{\zeta}_1(k) + \bar{\zeta}_1\big)\varepsilon_1^T(k)\mathscr{F}^T Z\mathscr{F}\varepsilon_0(k) + 2\big(\check{\zeta}_2(k) + \bar{\zeta}_2\big) \\
&\times \varepsilon_2^T(k)\mathscr{F}^T Z\mathscr{A}\vartheta(k) + 2\big(\check{\zeta}_2(k) + \bar{\zeta}_2\big)\varepsilon_2^T(k)\mathscr{F}^T Z \\
&\times \mathscr{W}\tilde{\xi}(k) + 2\big(\check{\zeta}_2(k) + \bar{\zeta}_2\big)\varepsilon_2^T(k)\mathscr{F}^T Z\mathscr{B}v(k) \\
&+ 2\big(\check{\zeta}_0(k) + \bar{\zeta}_0\big)\big(\check{\zeta}_2(k) + \bar{\zeta}_2\big)\varepsilon_2^T(k)\mathscr{F}^T Z\mathscr{F}\varepsilon_0(k) \\
&+ 2\big(\check{\zeta}_1(k) + \bar{\zeta}_1\big)\big(\check{\zeta}_2(k) + \bar{\zeta}_2\big)\varepsilon_2^T(k)\mathscr{F}^T Z\mathscr{F}\varepsilon_1(k)\Big\} \\
=&\mathbb{E}\Big\{\vartheta^T(k)\big(\mathscr{A}^T Z \mathscr{A} - Z\big)\vartheta(k) + \tilde{\xi}^T(k)\mathscr{W}^T Z \mathscr{W}\tilde{\xi}(k) \\
&+ v^T(k)\mathscr{B}^T Z \mathscr{B} v(k) + \bar{\zeta}_0\varepsilon_0^T(k)\mathscr{F}^T Z\mathscr{F}\varepsilon_0(k) \\
&+ \bar{\zeta}_1\varepsilon_1^T(k)\mathscr{F}^T Z\mathscr{F}\varepsilon_1(k) + \bar{\zeta}_2\varepsilon_2^T(k)\mathscr{F}^T Z\mathscr{F}\varepsilon_2(k) \\
&+ 2\tilde{\xi}^T(k)\mathscr{W}^T Z\mathscr{A}\vartheta(k) + 2v^T(k)\mathscr{B}^T Z\mathscr{A}\vartheta(k) \\
&+ 2v^T(k)\mathscr{B}^T Z\mathscr{W}\tilde{\xi}(k) + 2\bar{\zeta}_0\varepsilon_0^T(k)\mathscr{F}^T Z\mathscr{A}\vartheta(k) \\
&+ 2\bar{\zeta}_0\varepsilon_0^T(k)\mathscr{F}^T Z\mathscr{W}\tilde{\xi}(k) + 2\bar{\zeta}_0\varepsilon_0^T(k)\mathscr{F}^T Z\mathscr{B}v(k) \\
&+ 2\bar{\zeta}_1\varepsilon_1^T(k)\mathscr{F}^T Z\mathscr{A}\vartheta(k) + 2\bar{\zeta}_1\varepsilon_1^T(k)\mathscr{F}^T Z\mathscr{W}\tilde{\xi}(k) \\
&+ 2\bar{\zeta}_1\varepsilon_1^T(k)\mathscr{F}^T Z\mathscr{B}v(k) + 2\bar{\zeta}_2\varepsilon_2^T(k)\mathscr{F}^T Z\mathscr{A}\vartheta(k) \\
&+ 2\bar{\zeta}_2\varepsilon_2^T(k)\mathscr{F}^T Z\mathscr{W}\tilde{\xi}(k) + 2\bar{\zeta}_2\varepsilon_2^T(k)\mathscr{F}^T Z\mathscr{B}v(k)\Big\} \\
=&\mathbb{E}\Big\{\vartheta^T(k)\big(\mathscr{A}^T Z \mathscr{A} - Z + \psi_1 Z\big)\vartheta(k) + \tilde{\xi}^T(k) \\
&\times \mathscr{W}^T Z \mathscr{W}\tilde{\xi}(k) + v^T(k)\big(\mathscr{B}^T Z \mathscr{B} - \psi_2 I\big)v(k) \\
&+ \varepsilon_0^T(k)\big(\bar{\zeta}_0\mathscr{F}^T Z\mathscr{F} - \psi_3 I\big)\varepsilon_0(k) + \varepsilon_1^T(k)\big(\bar{\zeta}_1\mathscr{F}^T Z \\
&\times \mathscr{F} - \psi_4 I\big)\varepsilon_1(k) + \varepsilon_2^T(k)\big(\bar{\zeta}_2\mathscr{F}^T Z\mathscr{F} - \psi_5 I\big)\varepsilon_2(k) \\
&+ 2\tilde{\xi}^T(k)\mathscr{W}^T Z\mathscr{A}\vartheta(k) + 2v^T(k)\mathscr{B}^T Z\mathscr{A}\vartheta(k) \\
&+ 2v^T(k)\mathscr{B}^T Z\mathscr{W}\tilde{\xi}(k) + 2\bar{\zeta}_0\varepsilon_0^T(k)\mathscr{F}^T Z\mathscr{A}\vartheta(k) \\
&+ 2\bar{\zeta}_0\varepsilon_0^T(k)\mathscr{F}^T Z\mathscr{W}\tilde{\xi}(k) + 2\bar{\zeta}_0\varepsilon_0^T(k)\mathscr{F}^T Z\mathscr{B}v(k) \\
&+ 2\bar{\zeta}_1\varepsilon_1^T(k)\mathscr{F}^T Z\mathscr{A}\vartheta(k) + 2\bar{\zeta}_1\varepsilon_1^T(k)\mathscr{F}^T Z\mathscr{W}\tilde{\xi}(k) \\
&+ 2\bar{\zeta}_1\varepsilon_1^T(k)\mathscr{F}^T Z\mathscr{B}v(k) + 2\bar{\zeta}_2\varepsilon_2^T(k)\mathscr{F}^T Z\mathscr{A}\vartheta(k) \\
&+ 2\bar{\zeta}_2\varepsilon_2^T(k)\mathscr{F}^T Z\mathscr{W}\tilde{\xi}(k) + 2\bar{\zeta}_2\varepsilon_2^T(k)\mathscr{F}^T Z\mathscr{B}v(k) \\
&- \psi_1 V\big(\vartheta(k)\big) + \psi_2 v^T(k)v(k) + \psi_3\varepsilon_0^T(k)\varepsilon_0(k) \\
&+ \psi_4\varepsilon_1^T(k)\varepsilon_1(k) + \psi_5\varepsilon_2^T(k)\varepsilon_2(k)\Big\}.
\end{aligned} \tag{41}$$

It is inferred from (3) that

$$\begin{bmatrix}\vartheta(k) \\ \tilde{\xi}(k)\end{bmatrix}^T \begin{bmatrix}\bar{Q}_1 & \star \\ -\bar{Q}_2 & I\end{bmatrix} \begin{bmatrix}\vartheta(k) \\ \tilde{\xi}(k)\end{bmatrix} \leqslant 0. \tag{42}$$

Recalling (36), we obtain from (41)-(42) that

$$\begin{aligned}
&\mathbb{E}\left\{\Re V\big(\vartheta(k)\big)\right\} \\
\leqslant&\mathbb{E}\big\{\rho^T(k)\bar{\Psi}_1\rho(k)\big\} - \psi_1\mathbb{E}\big\{V\big(\vartheta(k)\big)\big\} \\
&+ \psi_2 v^T(k)v(k) + \bar{\psi}_3\varepsilon_0^T(k)\varepsilon_0(k) \\
&+ \psi_4\varepsilon_1^T(k)\varepsilon_1(k) + \psi_5\varepsilon_2^T(k)\varepsilon_2(k)
\end{aligned} \tag{43}$$

where

$$\rho(k) \triangleq \begin{bmatrix}\vartheta^T(k) & \tilde{\xi}^T(k) & v^T(k) & \varepsilon_0^T(k) & \varepsilon_1^T(k) & \varepsilon_2^T(k)\end{bmatrix}^T$$

This article has been accepted for publication in a future issue of this journal, but has not been fully edited. Content may change prior to final publication.
Citation information: DOI: 10.1109/TNNLS.2022.3209632, IEEE Transactions on Neural Networks and Learning Systems

$$\bar{\Psi}_1 \triangleq \begin{bmatrix} \bar{\Psi}_1^{11} & \star & \star & \star & \star & \star \\ \bar{\Psi}_1^{21} & \bar{\Psi}_1^{22} & \star & \star & \star & \star \\ \bar{\Psi}_1^{31} & \bar{\Psi}_1^{32} & \bar{\Psi}_1^{33} & \star & \star & \star \\ \bar{\Psi}_1^{41} & \bar{\Psi}_1^{42} & \bar{\Psi}_1^{43} & \bar{\Psi}_1^{44} & \star & \star \\ \mathbf{0} & \mathbf{0} & \mathbf{0} & \mathbf{0} & \bar{\Psi}_1^{55} & \star \\ \mathbf{0} & \mathbf{0} & \mathbf{0} & \mathbf{0} & \mathbf{0} & \bar{\Psi}_1^{66} \end{bmatrix}$$

$$\bar{\Psi}_1^{11} \triangleq (\varphi_1+\varphi_4+1)\mathscr{A}^T Z\mathscr{A} - Z + \psi_1 Z - \psi_6\bar{Q}_1$$
$$\bar{\Psi}_1^{22} \triangleq (\varphi_2+\varphi_5+1)\mathscr{W}^T Z\mathscr{W} - \psi_6 I$$
$$\bar{\Psi}_1^{33} \triangleq (\varphi_3+\varphi_6+1)\mathscr{B}^T Z\mathscr{B} - \psi_2 I$$
$$\bar{\Psi}_1^{44} \triangleq \bar{\zeta}_0^2\mathscr{F}^T Z\mathscr{F} - \psi_3 I, \quad \bar{\psi}_3 \triangleq \psi_3 + \bar{\zeta}_0$$
$$\bar{\Psi}_1^{55} \triangleq (\bar{\zeta}_1 + \frac{\bar{\zeta}_1^2}{\varphi_1} + \frac{\bar{\zeta}_1^2}{\varphi_2} + \frac{\bar{\zeta}_1^2}{\varphi_3})\mathscr{F}^T Z\mathscr{F} - \psi_4 I$$
$$\bar{\Psi}_1^{66} \triangleq (\bar{\zeta}_2 + \frac{\bar{\zeta}_2^2}{\varphi_4} + \frac{\bar{\zeta}_2^2}{\varphi_5} + \frac{\bar{\zeta}_2^2}{\varphi_6})\mathscr{F}^T Z\mathscr{F} - \psi_5 I$$
$$\bar{\Psi}_1^{21} \triangleq \mathscr{W}^T Z\mathscr{A} + \psi_6\bar{Q}_2, \quad \bar{\Psi}_1^{31} \triangleq \mathscr{B}^T Z\mathscr{A}$$
$$\bar{\Psi}_1^{32} \triangleq \mathscr{B}^T Z\mathscr{W}, \quad \bar{\Psi}_1^{41} \triangleq \bar{\zeta}_0\mathscr{F}^T Z\mathscr{A}$$
$$\bar{\Psi}_1^{42} \triangleq \bar{\zeta}_0\mathscr{F}^T Z\mathscr{W}, \quad \bar{\Psi}_1^{43} \triangleq \bar{\zeta}_0\mathscr{F}^T Z\mathscr{B}.$$

By applying the Schur Complement Lemma, it is easy to see that $\bar{\Psi}_1 < 0$ can be ensured by (37), which implies that

$$\begin{aligned} &\mathbb{E}\left\{\Re V\big(\vartheta(k)\big)\right\} \\ \leqslant& -\psi_1\mathbb{E}\big\{V\big(\vartheta(k)\big)\big\} + \psi_2 v^T(k)v(k) \\ &+ \bar{\psi}_3\varepsilon_0^T(k)\varepsilon_0(k) + \psi_4\varepsilon_1^T(k)\varepsilon_1(k) \\ &+ \psi_5\varepsilon_2^T(k)\varepsilon_2(k). \end{aligned} \tag{44}$$

Denoting $\gamma_1(k) \triangleq \psi_2\bar{v} + (\kappa\bar{\psi}_3 + 5\psi_4 + \psi_5)\varpi_2(k)$, we have from (16) and (33) that

$$\gamma_1(k) \leqslant \psi_2\bar{v} + (\kappa\bar{\psi}_3 + 5\psi_4 + \psi_5)\sqrt{\sum_{\imath=1}^{h}\big(\frac{\pi_\imath d}{g}\big)^2} \triangleq \gamma_2 \tag{45}$$

which yields

$$\mathbb{E}\left\{\Re V\big(\vartheta(k)\big)\right\} \leqslant -\psi_1\mathbb{E}\big\{V\big(\vartheta(k)\big)\big\} + \gamma_2. \tag{46}$$

For any scalar $\hbar > 1$, it follows that

$$\begin{aligned} &\mathbb{E}\left\{\hbar^{k+1}V\big(\vartheta(k+1)\big)\right\} - \mathbb{E}\left\{\hbar^k V\big(\vartheta(k)\big)\right\} \\ =&\hbar^{k+1}\mathbb{E}\left\{V\big(\vartheta(k+1)\big) - V\big(\vartheta(k)\big)\right\} \\ &+ \hbar^{k+1}\mathbb{E}\left\{V\big(\vartheta(k)\big)\right\} - \hbar^k\mathbb{E}\left\{V\big(\vartheta(k)\big)\right\} \\ =&\hbar^{k+1}\mathbb{E}\left\{\Re V\big(\vartheta(k)\big)\right\} + \hbar^k(\hbar-1)\mathbb{E}\left\{V\big(\vartheta(k)\big)\right\} \\ \leqslant&\hbar^{k+1}\Big(-\psi_1\mathbb{E}\big\{V\big(\vartheta(k)\big)\big\} + \gamma_2\Big) \\ &+ \hbar^k(\hbar-1)\mathbb{E}\left\{V\big(\vartheta(k)\big)\right\} \\ =&\hbar^k(\hbar-1-\hbar\psi_1)\mathbb{E}\left\{V\big(\vartheta(k)\big)\right\} + \hbar^k\gamma_2 \\ =&\hbar^k p(\hbar)\mathbb{E}\left\{V\big(\vartheta(k)\big)\right\} + \hbar^{k+1}\gamma_2 \end{aligned} \tag{47}$$

where

$$p(\hbar) \triangleq \hbar - 1 - \hbar\psi_1.$$

For any integer $t \geqslant 0$, taking cumulative summation for the left- and right-hand sides of inequality (47) from 0 to $t-1$ with respect to k leads to

$$\begin{aligned} &\hbar^t\mathbb{E}\left\{V\big(\vartheta(t)\big)\right\} - \mathbb{E}\left\{V\big(\vartheta(0)\big)\right\} \\ \leqslant& p(\hbar)\sum_{k=0}^{t-1}\hbar^k\mathbb{E}\left\{V\big(\vartheta(k)\big)\right\} + \frac{\hbar(1-\hbar^t)}{1-\hbar}\gamma_2. \end{aligned} \tag{48}$$

Noticing $p(1) = -\psi_1 < 0$ and $\lim_{\hbar\to\infty} p(\hbar) = +\infty$, we conclude that there exists a scalar $\hbar_0 > 1$ such that $p(\hbar_0) = 0$. Hence, we have

$$\begin{aligned} &\hbar_0^t\mathbb{E}\left\{V\big(\vartheta(t)\big)\right\} - \mathbb{E}\left\{V\big(\vartheta(0)\big)\right\} \\ \leqslant&\frac{\hbar_0(1-\hbar_0^t)}{1-\hbar_0}\gamma_2 \end{aligned} \tag{49}$$

and

$$\begin{aligned} &\mathbb{E}\left\{V\big(\vartheta(t)\big)\right\} \\ \leqslant&\frac{1}{\hbar_0^t}\mathbb{E}\left\{V\big(\vartheta(0)\big)\right\} + \frac{\hbar_0(1-\hbar_0^t)}{\hbar_0^t(1-\hbar_0)}\gamma_2 \end{aligned} \tag{50}$$

which, together with (39), indicates that

$$\begin{aligned} &\mathbb{E}\left\{\|\vartheta(t)\|^2\right\} \\ \leqslant&\frac{1}{\lambda_{\min}(Z)}\mathbb{E}\left\{V\big(\vartheta(t)\big)\right\} \\ \leqslant&\frac{\mathbb{E}\left\{V\big(\vartheta(0)\big)\right\}}{\lambda_{\min}(Z)\hbar_0^t} + \frac{\hbar_0(1-\hbar_0^t)}{\lambda_{\min}(Z)\hbar_0^t(1-\hbar_0)}\gamma_2. \end{aligned} \tag{51}$$

Denoting

$$\gamma_3(t) \triangleq \frac{\hbar_0(1-\hbar_0^t)}{\lambda_{\min}(Z)\hbar_0^t(1-\hbar_0)}\gamma_2,$$

we obtain

$$\gamma = \lim_{t\to+\infty}\gamma_3(t) = \frac{\gamma_2}{\lambda_{\min}(Z)\psi_1}. \tag{52}$$

Letting

$$\alpha \triangleq \hbar_0^{-1}, \quad \beta \triangleq \frac{\mathbb{E}\left\{V\big(\vartheta(0)\big)\right\}}{\lambda_{\min}(Z)},$$

we derive from Definition 1 that the dynamics of the augmented system (13) is exponentially ultimately bounded in mean-square sense and the asymptotic upper bound is given by

$$\gamma = \frac{\psi_2\bar{v} + (\kappa\psi_3 + \kappa\bar{\zeta}_0 + 5\psi_4 + \psi_5)\sqrt{\sum_{\imath=1}^{h}\big(\frac{\pi_\imath d}{g}\big)^2}}{\lambda_{\min}(Z)\psi_1}.$$

The proof is now complete. ■

E. Design of PIO

In this subsection, the PIO is devised by solving two optimization problems so as to achieve certain performance indices.

OP 1: The first optimization problem is to minimize the ultimate bound of the state estimation error dynamics for the sake of obtaining the best estimation performance. Such an optimization problem is tackled in Theorem 3.

Theorem 3: Let the positive scalars $\acute{\varphi}_1$, $\acute{\varphi}_2$, $\acute{\varphi}_3$, $\acute{\varphi}_4$, $\acute{\varphi}_5$, $\acute{\varphi}_6$ and scalar $\acute{\psi}_1$ $(0 < \acute{\psi}_1 < 1)$ be given. Suppose that there exist positive scalars $\acute{\psi}_2$, $\acute{\psi}_3$, $\acute{\psi}_4$, $\acute{\psi}_5$, $\acute{\psi}_6$ and positive definite

This article has been accepted for publication in a future issue of this journal, but has not been fully edited. Content may change prior to final publication.
Citation information: DOI: 10.1109/TNNLS.2022.3209632, IEEE Transactions on Neural Networks and Learning Systems

matrices $\acute{Z}_1$, $\acute{Z}_2$, matrices $\acute{F}_1$, $\acute{F}_2$, $\acute{F}_3$ satisfying the following inequalities:

$$\begin{cases} \Psi_2 = \begin{bmatrix} \Psi_2^1 & \star \\ \Psi_2^3 & \Psi_2^3 \end{bmatrix} < 0 & \text{(53a)} \\ \acute{Z} \geqslant I & \text{(53b)} \end{cases}$$

where

$$\Psi_2^1 \triangleq \text{diag}\{\Psi_2^4,\ -\acute{\psi}_2 I,\ -\acute{\psi}_3 I,\ -\acute{\psi}_4 I,\ -\acute{\psi}_5 I,\}$$

$$\Psi_2^2 \triangleq \begin{bmatrix} \acute{\mathcal{A}} & \acute{\mathcal{W}} & \acute{\mathcal{B}} & \bar{\zeta}_0 \acute{\mathcal{F}} & \mathbf{0} & \mathbf{0} \\ \Psi_2^5 & \mathbf{0} & \mathbf{0} & \mathbf{0} & \mathbf{0} & \mathbf{0} \\ \mathbf{0} & \Psi_2^6 & \mathbf{0} & \mathbf{0} & \mathbf{0} & \mathbf{0} \\ \mathbf{0} & \mathbf{0} & \Psi_2^7 & \mathbf{0} & \mathbf{0} & \mathbf{0} \\ \mathbf{0} & \mathbf{0} & \mathbf{0} & \mathbf{0} & \Psi_2^8 & \mathbf{0} \\ \mathbf{0} & \mathbf{0} & \mathbf{0} & \mathbf{0} & \mathbf{0} & \Psi_2^9 \end{bmatrix}$$

$$\Psi_2^3 \triangleq -I_6 \otimes \acute{Z},\ \Psi_2^4 \triangleq \begin{bmatrix} -\acute{\psi}_1 \acute{Z} - \acute{\psi}_6 \bar{Q}_1 & \star \\ \acute{\psi}_6 \bar{Q}_2 & -\acute{\psi}_6 I \end{bmatrix}$$

$$\Psi_2^5 \triangleq \sqrt{\acute{\varphi}_1 + \acute{\varphi}_4}\acute{\mathcal{A}}, \quad \Psi_2^6 \triangleq \sqrt{\acute{\varphi}_2 + \acute{\varphi}_5}\acute{\mathcal{W}}$$

$$\Psi_2^7 \triangleq \sqrt{\acute{\varphi}_3 + \acute{\varphi}_6}\acute{\mathcal{B}}, \quad \Psi_2^8 \triangleq \sqrt{\bar{\zeta}_1 + \frac{\bar{\zeta}_1^2}{\acute{\varphi}_1} + \frac{\bar{\zeta}_1^2}{\acute{\varphi}_2} + \frac{\bar{\zeta}_1^2}{\acute{\varphi}_3}}\acute{\mathcal{F}}$$

$$\Psi_2^9 \triangleq \sqrt{\bar{\zeta}_2 + \frac{\bar{\zeta}_2^2}{\acute{\varphi}_4} + \frac{\bar{\zeta}_2^2}{\acute{\varphi}_5} + \frac{\bar{\zeta}_2^2}{\acute{\varphi}_6}}\acute{\mathcal{F}}, \quad \acute{Z} \triangleq \text{diag}\left\{\acute{Z}_1,\ \acute{Z}_2\right\}$$

$$\acute{\mathcal{A}} \triangleq \begin{bmatrix} \acute{Z}_1 A - \acute{F}_2 C & -\acute{F}_1 \\ \acute{F}_3 C & \acute{Z}_2 \end{bmatrix}, \quad \acute{\mathcal{W}} \triangleq \begin{bmatrix} \acute{Z}_1 W \\ \mathbf{0} \end{bmatrix}$$

$$\acute{\mathcal{B}} \triangleq \begin{bmatrix} \acute{Z}_1 B \\ \mathbf{0} \end{bmatrix}, \qquad \acute{\mathcal{F}} \triangleq \begin{bmatrix} -\acute{F}_2 \\ \acute{F}_3 \end{bmatrix}.$$

Then, the dynamics of the augmented system (13) is exponentially mean-square ultimately bounded. Moreover, in mean-square sense, the decay rate of $\|\vartheta(k)\|^2$ is $\acute{\psi}_1$ and the minimum of the asymptotic upper bound of $\|\vartheta(k)\|^2$ can be obtained by solving the following minimization problem:

$$\begin{aligned} \min \quad & \acute{\psi}_2 \bar{v} + (\kappa \acute{\psi}_3 + \kappa \bar{\zeta}_0 + 5\acute{\psi}_4 + \acute{\psi}_5)\sqrt{\sum_{\imath=1}^{h} \left(\frac{\pi_\imath d}{g}\right)^2} \\ & \text{subject to} \ \ \text{(53a) and (53b).} \end{aligned} \tag{54}$$

In addition, the gains of PIO can be derived by:

$$F_1 = \acute{Z}_1^{-1}\acute{F}_1, \quad F_2 = \acute{Z}_1^{-1}\acute{F}_2, \quad F_3 = \acute{Z}_2^{-1}\acute{F}_3. \tag{55}$$

Proof: For the reason of notation uniformity, by letting $\acute{\psi}_1 = 1 - \psi_1$ and $\acute{Z} = Z$, we have

$$\Psi_2^1 = \Psi_1^1. \tag{56}$$

Noting

$$\acute{F}_1 = \acute{Z}_1 F_1, \quad \acute{F}_2 = \acute{Z}_1 F_2, \quad \acute{F}_3 = \acute{Z}_2 F_3 \tag{57}$$

we perform the congruence transformation to (37) by $\text{diag}\{I_6 \otimes I,\ I_6 \otimes \acute{Z}\}$ to produce $\Psi_1 < 0$, which proves that the exponentially mean-square ultimate boundedness of the augmented system (13) is guaranteed by (53a).

It is inferred from the equation $p(\hbar_0) = 0$ that

$$\acute{\psi}_1 = \frac{1}{\hbar_0}, \tag{58}$$

which gives rise to

$$\begin{aligned} & \mathbb{E}\left\{V\big(\vartheta(k)\big)\right\} \\ \leqslant & \frac{1}{1-\acute{\psi}_1}\left(\acute{\psi}_2 \bar{v} + (\kappa\acute{\psi}_3 + \kappa\bar{\zeta}_0 + 5\acute{\psi}_4 + \acute{\psi}_5)\sqrt{\sum_{\imath=1}^{h}\left(\frac{\pi_\imath d}{g}\right)^2}\right) \\ & + \acute{\psi}_1^k \mathbb{E}\left\{V\big(\vartheta(0)\big)\right\}. \end{aligned} \tag{59}$$

Next, it follows readily from (51) and (53b) that

$$\begin{aligned} & \mathbb{E}\left\{\|\vartheta(k)\|^2\right\} \\ \leqslant & \frac{1}{1-\acute{\psi}_1}\left(\acute{\psi}_2 \bar{v} + (\kappa\acute{\psi}_3 + \kappa\bar{\zeta}_0 + 5\acute{\psi}_4 + \acute{\psi}_5)\sqrt{\sum_{\imath=1}^{h}\left(\frac{\pi_\imath d}{g}\right)^2}\right) \\ & + \acute{\psi}_1^k \mathbb{E}\left\{V\big(\vartheta(0)\big)\right\}. \end{aligned} \tag{60}$$

Thus, the asymptotic bound of $\|\vartheta(k)\|^2$ (in mean-square sense) is minimized by solving the optimization problem (54). The proof is now complete. ■

OP 2: The second optimization problem is to optimize the decay rate of the state estimation error dynamics with aim to achieve the fastest convergence. Such an optimization problem is addressed in Theorem 4.

Theorem 4: Let the positive scalars $\grave{\varphi}_1$, $\grave{\varphi}_2$, $\grave{\varphi}_3$, $\grave{\varphi}_4$, $\grave{\varphi}_5$, $\grave{\varphi}_6$ be given. Suppose that there exist positive scalars $\grave{\psi}_1$, $\grave{\psi}_2$, $\grave{\psi}_3$, $\grave{\psi}_4$, $\grave{\psi}_5$, $\grave{\psi}_6$ and positive definite matrices $\grave{Z}_1$, $\grave{Z}_2$, $\breve{Z}$, matrices $\grave{F}_1$, $\grave{F}_2$, $\grave{F}_3$ satisfying the following inequalities:

$$\begin{cases} \Psi_3 = \begin{bmatrix} \Psi_3^1 & \star \\ \Psi_3^2 & \Psi_3^3 \end{bmatrix} < 0 & \text{(61a)} \\ \Psi_4 = \begin{bmatrix} \Psi_4^1 & \star \\ \Psi_4^2 & \Psi_4^3 \end{bmatrix} < 0 & \text{(61b)} \\ \grave{Z} \geqslant I & \text{(61c)} \end{cases}$$

where

$$\Psi_3^1 \triangleq \text{diag}\{\Psi_3^4,\ -\grave{\psi}_2 I,\ -\grave{\psi}_3 I,\ -\grave{\psi}_4 I,\ -\grave{\psi}_5 I,\}$$

$$\Psi_3^2 \triangleq \begin{bmatrix} \grave{\mathcal{A}} & \grave{\mathcal{W}} & \grave{\mathcal{B}} & \bar{\zeta}_0 \grave{\mathcal{F}} & \mathbf{0} & \mathbf{0} \\ \Psi_3^5 & \mathbf{0} & \mathbf{0} & \mathbf{0} & \mathbf{0} & \mathbf{0} \\ \mathbf{0} & \Psi_3^6 & \mathbf{0} & \mathbf{0} & \mathbf{0} & \mathbf{0} \\ \mathbf{0} & \mathbf{0} & \Psi_3^7 & \mathbf{0} & \mathbf{0} & \mathbf{0} \\ \mathbf{0} & \mathbf{0} & \mathbf{0} & \mathbf{0} & \Psi_3^8 & \mathbf{0} \\ \mathbf{0} & \mathbf{0} & \mathbf{0} & \mathbf{0} & \mathbf{0} & \Psi_3^9 \end{bmatrix}$$

$$\Psi_3^3 \triangleq -I_6 \otimes \grave{Z},\ \Psi_3^4 \triangleq \begin{bmatrix} -\grave{Z} + \breve{Z} - \grave{\psi}_6 \bar{Q}_1 & \star \\ \grave{\psi}_6 \bar{Q}_2 & -\grave{\psi}_6 I \end{bmatrix}$$

$$\Psi_3^5 \triangleq \sqrt{\grave{\varphi}_1 + \grave{\varphi}_4}\grave{\mathcal{A}}, \quad \Psi_3^6 \triangleq \sqrt{\grave{\varphi}_2 + \grave{\varphi}_5}\grave{\mathcal{W}}$$

$$\Psi_3^7 \triangleq \sqrt{\grave{\varphi}_3 + \grave{\varphi}_6}\grave{\mathcal{B}}, \quad \Psi_3^8 \triangleq \sqrt{\bar{\zeta}_1 + \frac{\bar{\zeta}_1^2}{\grave{\varphi}_1} + \frac{\bar{\zeta}_1^2}{\grave{\varphi}_2} + \frac{\bar{\zeta}_1^2}{\grave{\varphi}_3}}\grave{\mathcal{F}}$$

$$\Psi_3^9 \triangleq \sqrt{\bar{\zeta}_2 + \frac{\bar{\zeta}_2^2}{\grave{\varphi}_4} + \frac{\bar{\zeta}_2^2}{\grave{\varphi}_5} + \frac{\bar{\zeta}_2^2}{\grave{\varphi}_6}}\grave{\mathcal{F}}, \quad \grave{Z} \triangleq \text{diag}\left\{\grave{Z}_1,\ \grave{Z}_2\right\}$$

$$\Psi_4^1 \triangleq -\breve{Z}, \quad \Psi_4^2 \triangleq \grave{\psi}_1 I, \quad \Psi_4^3 \triangleq \grave{Z} - 2I$$

$$\grave{\mathcal{A}} \triangleq \begin{bmatrix} \grave{Z}_1 A - \grave{F}_2 C & -\grave{F}_1 \\ \grave{F}_3 C & \grave{Z}_2 \end{bmatrix}, \quad \grave{\mathcal{W}} \triangleq \begin{bmatrix} \grave{Z}_1 W \\ \mathbf{0} \end{bmatrix}$$

$$\grave{\mathcal{B}} \triangleq \begin{bmatrix} \grave{Z}_1 B \\ \mathbf{0} \end{bmatrix}, \qquad \grave{\mathcal{F}} \triangleq \begin{bmatrix} -\grave{F}_2 \\ \grave{F}_3 \end{bmatrix}.$$

This article has been accepted for publication in a future issue of this journal, but has not been fully edited. Content may change prior to final publication.
Citation information: DOI: 10.1109/TNNLS.2022.3209632, IEEE Transactions on Neural Networks and Learning Systems

Then, the dynamics of the augmented system (13) is exponentially mean-square ultimately bounded. Moreover, in mean-square sense, the maximum decay rate of $\|\vartheta(k)\|^2$ is derived by solving the following maximization problem:

$$\begin{aligned} &\max \ \ \grave{\psi}_1 \\ &\text{subject to} \ \ (61a)-(61c). \end{aligned} \tag{62}$$

In addition, the gains of PIO are derived by:

$$F_1=\grave{Z}_1^{-1}\grave{F}_1, \quad F_2=\grave{Z}_1^{-1}\grave{F}_2, \quad F_3=\grave{Z}_2^{-1}\grave{F}_3. \tag{63}$$

Proof: Pre-multiplying and post-multiplying (37) by $\text{diag}\{I_6\otimes I,\ I_6\otimes \grave{Z}\}$ and taking variable substitutions

$$\begin{aligned} \grave{F}_1=&\grave{Z}_1F_1, \quad \grave{F}_2=\grave{Z}_1F_2 \\ \grave{F}_3=&\grave{Z}_2F_3, \quad \grave{W}=Z, \end{aligned} \tag{64}$$

one has

$$\Psi_5=\begin{bmatrix}\Psi_1^1 & \star\\ \Psi_3^2 & \Psi_3^3\end{bmatrix}<0. \tag{65}$$

Substituting $\grave{\psi}_1=\sqrt{\psi_1}$ into (65) gives

$$\Psi_6=\begin{bmatrix}\Psi_6^1 & \star\\ \Psi_3^2 & \Psi_3^3\end{bmatrix}<0 \tag{66}$$

where

$$\begin{aligned} \Phi_6^1 \triangleq&\text{diag}\{\Psi_6^2,\ -\grave{\psi}_2 I,\ -\grave{\psi}_3 I,\ -\grave{\psi}_4 I,\ -\grave{\psi}_5 I,\}\\ \Psi_6^2 \triangleq&\begin{bmatrix}-\grave{Z}+\grave{\psi}_1^2\grave{Z}-\grave{\psi}_6\bar{Q}_1 & \star\\ \grave{\psi}_6\bar{Q}_2 & -\grave{\psi}_6 I\end{bmatrix}. \end{aligned}$$

Furthermore, it follows from

$$(\grave{Z}-I)\grave{Z}^{-1}(\grave{Z}-I)\geqslant 0 \tag{67}$$

that

$$-\grave{Z}^{-1}\leqslant \grave{Z}-2I. \tag{68}$$

In view of (61b), one confirms

$$\begin{bmatrix}-\check{Z} & \star\\ \grave{\psi}_1 I & -\grave{Z}^{-1}\end{bmatrix}<0. \tag{69}$$

By means of the Schur Complement Lemma, one finally obtain

$$-\check{Z}+\grave{\psi}_1^2\grave{Z}<0, \tag{70}$$

which means that (66) is ensured by (61a). Thus, according to Definition 1, the augmented system (13) is exponentially ultimately bounded in mean-square sense.

Along the similar line to the proof of Theorem 2, the following inequality can be obtained:

$$\begin{aligned} &\mathbb{E}\left\{\|\vartheta(k)\|^2\right\}\\ \leqslant&\frac{1}{\grave{\psi}_1^2}\left(\grave{\psi}_2\bar{v}+(\kappa\grave{\psi}_3+\kappa\bar{\zeta}_0+5\grave{\psi}_4+\grave{\psi}_5)\sqrt{\sum_{\imath=1}^{h}\left(\frac{\pi_\imath d}{g}\right)^2}\right)\\ &+(1-\grave{\psi}_1^2)^k\mathbb{E}\left\{V\big(\vartheta(0)\big)\right\}, \end{aligned} \tag{71}$$

based on which the decay rate of $\|\vartheta(k)\|^2$ (in mean-square sense) is thus determined by $1-\grave{\psi}_1^2$. Obviously, after the maximization problem (62) is solved, the optimum decay rate can be obtained accordingly, and this completes the proof. ■

Remark 5: So far, the partial-neurons-based PIO design problem has been solved for ANNs subject to randomly occurring packet dropout and bounded disturbance under the MDES. In comparison to the available PIO design literature on ANNs, our primary results own the following distinctive merits: 1) the devised PIO is novel as the observer is dedicatedly constructed to estimate the state of all neurons only based on partially accessible neuron measurements; 2) the adopted MDES plays a dominant role in enhancing the reliability of signal transmission (as compared with the traditional uniform-quantization-based encoding mechanism); and 3) the established theoretical framework is suited for quantitatively analyzing the influences from the packet-dropout probabilities and the decoding errors on the estimation performance.

F. Design of Luenberger Observer

In this subsection, the design issue of the Luenberger observer (a special case of the PIO developed in this paper) will be addressed in order to achieve the best estimation performance or the fastest convergence.

The Luenberger observer is constructed as follows:

$$\hat{x}(k+1)=A\hat{x}(k)+W\xi\big(\hat{x}(k)\big)+F_4\big(\check{y}(k)-C\hat{x}(k)\big) \tag{72}$$

with F_4 being the gain matrix and, accordingly, the dynamics of estimation error can be formulated as:

$$\begin{aligned} \tilde{x}(k+1)=&\mathfrak{A}\tilde{x}(k)+W\tilde{\xi}(k)+Bv(k)+\big(\check{\zeta}_0(k)+\bar{\zeta}_0\big)\mathfrak{F}_4\varepsilon_0(k)\\ &+\big(\check{\zeta}_1(k)+\bar{\zeta}_1\big)\mathfrak{F}_4\varepsilon_1(k)+\big(\check{\zeta}_2(k)+\bar{\zeta}_2\big)\mathfrak{F}_4\varepsilon_2(k) \end{aligned} \tag{73}$$

where

$$\mathfrak{A}\triangleq A-F_4C, \quad \mathfrak{F}_4\triangleq -F_4.$$

The following corollaries are easily accessible from Theorems 2-4.

Corollary 1: Let the positive scalars $\check{\varphi}_1$, $\check{\varphi}_2$, $\check{\varphi}_3$, $\check{\varphi}_4$, $\check{\varphi}_5$, $\check{\varphi}_6$ and scalar $\check{\psi}_1$ $(0<\check{\psi}_1<1)$ be given. Suppose that there exist positive scalars $\check{\psi}_2$, $\check{\psi}_3$, $\check{\psi}_4$, $\check{\psi}_5$, $\check{\psi}_6$ and positive definite matrix $\check{Z}$, matrix $\check{\mathfrak{F}}_4$ satisfying the following inequalities:

$$\begin{cases} \Omega_1=\begin{bmatrix}\Omega_1^1 & \star\\ \Omega_1^2 & \Omega_1^3\end{bmatrix}<0 & (74a)\\ \check{Z}\geqslant I & (74b)\end{cases}$$

where

$$\begin{aligned} \Omega_1^1 \triangleq&\text{diag}\{\Omega_1^4,\ -\check{\psi}_2 I,\ -\check{\psi}_3 I,\ -\check{\psi}_4 I,\ -\check{\psi}_5 I,\}\\ \Omega_1^2 \triangleq&\begin{bmatrix}\check{\mathcal{A}} & \check{\mathcal{W}} & \check{\mathcal{B}} & \bar{\zeta}_0\check{\mathfrak{F}}_4 & \mathbf{0} & \mathbf{0}\\ \Omega_1^5 & \mathbf{0} & \mathbf{0} & \mathbf{0} & \mathbf{0} & \mathbf{0}\\ \mathbf{0} & \Omega_1^6 & \mathbf{0} & \mathbf{0} & \mathbf{0} & \mathbf{0}\\ \mathbf{0} & \mathbf{0} & \Omega_1^7 & \mathbf{0} & \mathbf{0} & \mathbf{0}\\ \mathbf{0} & \mathbf{0} & \mathbf{0} & \mathbf{0} & \Omega_1^8 & \mathbf{0}\\ \mathbf{0} & \mathbf{0} & \mathbf{0} & \mathbf{0} & \mathbf{0} & \Omega_1^9\end{bmatrix}\\ \Omega_1^3 \triangleq&-I_6\otimes\check{Z},\ \Omega_1^4\triangleq\begin{bmatrix}-\check{\psi}_1\check{Z}-\check{\psi}_6Q_1 & \star\\ \check{\psi}_6Q_2 & -\check{\psi}_6 I\end{bmatrix}\\ \Omega_1^5 \triangleq&\sqrt{\check{\varphi}_1+\check{\varphi}_4}\check{\mathcal{A}}, \quad \Omega_1^6\triangleq\sqrt{\check{\varphi}_2+\check{\varphi}_5}\check{\mathcal{W}}\\ \Omega_1^7 \triangleq&\sqrt{\check{\varphi}_3+\check{\varphi}_6}\check{\mathcal{B}}, \quad \Omega_1^8\triangleq\sqrt{\bar{\zeta}_1+\frac{\bar{\zeta}_1^2}{\check{\varphi}_1}+\frac{\bar{\zeta}_1^2}{\check{\varphi}_2}+\frac{\bar{\zeta}_1^2}{\check{\varphi}_3}}\check{\mathfrak{F}}_4 \end{aligned}$$

This article has been accepted for publication in a future issue of this journal, but has not been fully edited. Content may change prior to final publication.
Citation information: DOI: 10.1109/TNNLS.2022.3209632, IEEE Transactions on Neural Networks and Learning Systems

$$\Omega_1^9 \triangleq \sqrt{\bar{\zeta}_2 + \frac{\bar{\zeta}_2^2}{\check{\varphi}_4} + \frac{\bar{\zeta}_2^2}{\check{\varphi}_5} + \frac{\bar{\zeta}_2^2}{\check{\varphi}_6}}\check{\mathfrak{F}}_4, \quad \check{\mathcal{A}} \triangleq \check{Z}A + \check{\mathfrak{F}}_4 C$$
$$\check{\mathcal{W}} \triangleq \check{Z}W, \quad \check{\mathcal{B}} \triangleq \check{Z}B.$$

Then, the dynamics of the augmented system (73) is exponentially mean-square ultimately bounded. Moreover, in mean-square sense, the decay rate of $\|\tilde{x}(k)\|^2$ is $\check{\psi}_1$ and the minimum of the asymptotic upper bound of $\|\tilde{x}(k)\|^2$ can be obtained by solving the following minimization problem:

$$\begin{aligned} \min \quad & \check{\psi}_2\bar{v} + (\kappa\check{\psi}_3 + \kappa\bar{\zeta}_0 + 5\check{\psi}_4 + \check{\psi}_5)\sqrt{\sum_{i=1}^{h}\left(\frac{\pi_i d}{g}\right)^2} \\ \text{subject to} \quad & \text{(74a) and (74b).} \end{aligned} \tag{75}$$

In addition, the gain of Luenberger observer can be derived by

$$F_4 = -\check{Z}_1^{-1}\check{\mathfrak{F}}_4. \tag{76}$$

Corollary 2: Let the positive scalars $\hat{\varphi}_1$, $\hat{\varphi}_2$, $\hat{\varphi}_3$, $\hat{\varphi}_4$, $\hat{\varphi}_5$, $\hat{\varphi}_6$ be given. Suppose that there exist positive scalars $\hat{\psi}_1$, $\hat{\psi}_2$, $\hat{\psi}_3$, $\hat{\psi}_4$, $\hat{\psi}_5$, $\hat{\psi}_6$ and positive definite matrices $\hat{Z}$, $\bar{Z}$, matrix $\tilde{\mathfrak{F}}_4$ satisfying the following inequalities:

$$\begin{cases} \Omega_2 = \begin{bmatrix} \Omega_2^1 & \star \\ \Omega_2^2 & \Omega_2^3 \end{bmatrix} < 0 & \text{(77a)} \\ \Omega_3 = \begin{bmatrix} \Omega_3^1 & \star \\ \Omega_3^2 & \Omega_3^3 \end{bmatrix} < 0 & \text{(77b)} \\ \hat{Z} \geqslant I & \text{(77c)} \end{cases}$$

where

$$\Omega_2^1 \triangleq \text{diag}\{\Omega_2^4,\ -\hat{\psi}_2 I,\ -\hat{\psi}_3 I,\ -\hat{\psi}_4 I,\ -\hat{\psi}_5 I\}$$
$$\Omega_2^2 \triangleq \begin{bmatrix} \hat{\mathcal{A}} & \hat{\mathcal{W}} & \hat{\mathcal{B}} & \bar{\zeta}_0\tilde{\mathfrak{F}}_4 & \mathbf{0} & \mathbf{0} \\ \Omega_2^5 & \mathbf{0} & \mathbf{0} & \mathbf{0} & \mathbf{0} & \mathbf{0} \\ \mathbf{0} & \Omega_2^6 & \mathbf{0} & \mathbf{0} & \mathbf{0} & \mathbf{0} \\ \mathbf{0} & \mathbf{0} & \Omega_2^7 & \mathbf{0} & \mathbf{0} & \mathbf{0} \\ \mathbf{0} & \mathbf{0} & \mathbf{0} & \mathbf{0} & \Omega_2^8 & \mathbf{0} \\ \mathbf{0} & \mathbf{0} & \mathbf{0} & \mathbf{0} & \mathbf{0} & \Omega_2^9 \end{bmatrix}$$
$$\Omega_2^3 \triangleq -I_6 \otimes \hat{Z},\ \Omega_2^4 \triangleq \begin{bmatrix} -\hat{Z} + \tilde{Z} - \hat{\psi}_6 Q_1 & \star \\ \hat{\psi}_6 Q_2 & -\hat{\psi}_6 I \end{bmatrix}$$
$$\Omega_2^5 \triangleq \sqrt{\hat{\varphi}_1 + \hat{\varphi}_4}\hat{\mathcal{A}}, \quad \Omega_2^6 \triangleq \sqrt{\hat{\varphi}_2 + \hat{\varphi}_5}\hat{\mathcal{W}}$$
$$\Omega_2^7 \triangleq \sqrt{\hat{\varphi}_3 + \hat{\varphi}_6}\hat{\mathcal{B}}, \quad \Omega_2^8 \triangleq \sqrt{\bar{\zeta}_1 + \frac{\bar{\zeta}_1^2}{\hat{\varphi}_1} + \frac{\bar{\zeta}_1^2}{\hat{\varphi}_2} + \frac{\bar{\zeta}_1^2}{\hat{\varphi}_3}}\hat{\mathfrak{F}}_4$$
$$\Omega_2^9 \triangleq \sqrt{\bar{\zeta}_2 + \frac{\bar{\zeta}_2^2}{\hat{\varphi}_4} + \frac{\bar{\zeta}_2^2}{\hat{\varphi}_5} + \frac{\bar{\zeta}_2^2}{\hat{\varphi}_6}}\hat{\mathfrak{F}}_4, \quad \hat{\mathcal{A}} \triangleq \hat{Z}A + \hat{\mathfrak{F}}_4 C$$
$$\hat{\mathcal{W}} \triangleq \hat{Z}W, \quad \hat{\mathcal{B}} \triangleq \hat{Z}B, \quad \Omega_3^1 \triangleq -\tilde{Z}$$
$$\Omega_3^2 \triangleq \hat{\psi}_1 I, \quad \Omega_3^3 \triangleq \hat{Z} - 2I.$$

Then, the dynamics of the augmented system (73) is exponentially mean-square ultimately bounded. Moreover, in mean-square sense, the maximum decay rate of $\|\tilde{x}(k)\|^2$ is derived by solving the following maximization problem:

$$\begin{aligned} \max \quad & \hat{\psi}_1 \\ \text{subject to} \quad & \text{(77a)} - \text{(77c)}. \end{aligned} \tag{78}$$

In addition, the gain of Luenberger observer is derived by:

$$F_4 = -\hat{Z}_1^{-1}\hat{\mathfrak{F}}_4. \tag{79}$$

IV. Numerical simulation

In this section, we leverage an illustrative simulation example to showcase the effectiveness and advantage of the presented observer design strategy.

The ANN with three neurons is considered in this section with the following parameters:

$$\begin{aligned} a_1 =& 0.281, \quad a_2 = 0.237, \quad a_3 = 0.306 \\ b_1 =& 0.11, \quad b_2 = 0.12, \quad b_3 = 0.13 \end{aligned}$$

and the connection weight matrix is set as

$$W = \begin{bmatrix} 0.5 & 0.4 & 0.3 \\ 0.3 & 0.2 & 0.1 \\ 0.1 & 0.2 & 0.3 \end{bmatrix}.$$

Additionally, the activation functions are given by

$$\begin{aligned} \xi_1\big(x_1(k)\big) =& 0.6\tanh\big(0.2x_1(k)\big) + 0.7x_1(k) \\ \xi_2\big(x_2(k)\big) =& 0.3\tanh\big(0.5x_2(k)\big) + 0.6x_2(k) \\ \xi_3\big(x_3(k)\big) =& 0.8\tanh\big(0.1x_3(k)\big) + 1.05x_3(k), \end{aligned}$$

which satisfies the sector bounded condition (3) with

$$\begin{aligned} \acute{q}_1 =& 0.82, \quad \grave{q}_1 = 0.7 \\ \acute{q}_2 =& 0.75, \quad \grave{q}_2 = 0.6 \\ \acute{q}_3 =& 1.13, \quad \grave{q}_3 = 1.05. \end{aligned}$$

It is assumed that the measurements of the first two neurons can be obtained and with

$$c_1 = 1.2 \quad c_2 = 0.1.$$

Moreover, the initial values of ANN (1) are set as $x_1(0) = 0.7$, $x_2(0) = -0.5$, $x_3(0) = 0.4$, and the initial values of PIO (8)-(10) and Luenberger observer (72) are chosen as zero. The external disturbances are given as

$$\begin{aligned} v_1(k) =& 0.1\sin(1.1k) \\ v_2(k) =& 0.2\sin(1.2k) \\ v_3(k) =& 0.3\sin(1.3k). \end{aligned}$$

A. State Estimation Effects of PIO

TABLE I: The comparison between Theorem 3 and Theorem 4

	Theorem 3 ($\check{\psi}_1 = 0.94$)	Theorem 4
Upper bound of $\|\tilde{x}(k)\|^2$	0.0518	0.0856
Setting-like time	6	4

In this subsection, we utilize the proposed PIO design scheme based on Theorem 3 and Theorem 4 to achieve different performances. The parameters of scalar quantizer (15) are selected as $d = 17$ and $g = 20$, and the decay rate $\check{\psi}_1$ in Theorem 3 is taken as 0.94. Accordingly, the gains of PIO can be calculated by solving the linear matrix inequalities in Theorem 3 and Theorem 4, respectively.

The state estimation results with respect to the different performances are shown in Figs. 3-5, where the blue lines depict the estimation error dynamics in the case of Theorem 3 and the red lines describe the estimation error dynamics

This article has been accepted for publication in a future issue of this journal, but has not been fully edited. Content may change prior to final publication.
Citation information: DOI: 10.1109/TNNLS.2022.3209632, IEEE Transactions on Neural Networks and Learning Systems

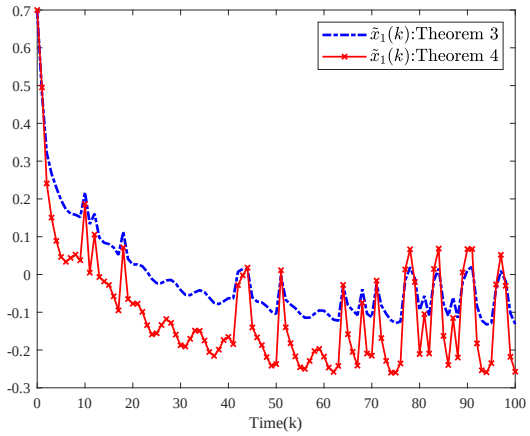

Fig. 3: Trajectories of $\tilde{x}_1(k)$ subject to *Theorem 3* and *Theorem 4*.

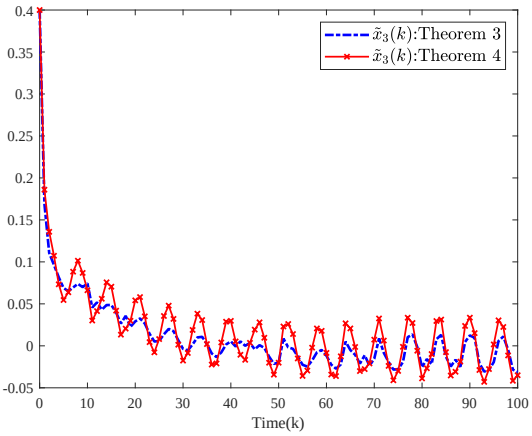

Fig. 5: Trajectories of $\tilde{x}_3(k)$ subject to *Theorem 3* and *Theorem 4*.

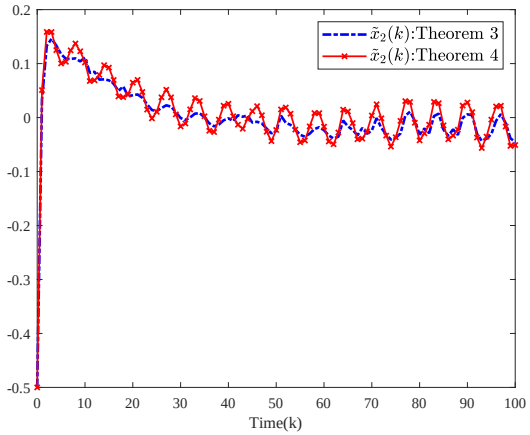

Fig. 4: Trajectories of $\tilde{x}_2(k)$ subject to *Theorem 3* and *Theorem 4*.

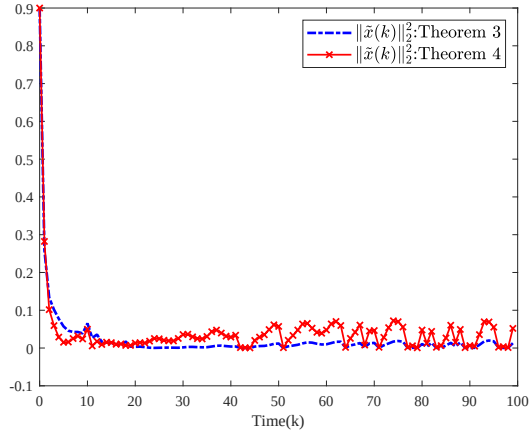

Fig. 6: Trajectories of $\|\tilde{x}(k)\|^2$ subject to *Theorem 3* and *Theorem 4*.

subject to Theorem 4. Obviously, by applying Theorem 3 and Theorem 4, the obtained PIO performs quite well. Additionally, to further elucidate the conclusion on different performance indices presented in Theorem 3 and Theorem 4, the upper bound of the estimation error and the settling-like times (the time required for the estimation error dynamics to reach and remain within the "steady-state region") are shown in Table I, respectively. From Figs. 3-5 and Table I, we can conclude that Theorem 3 contributes to a smaller upper bound of estimation errors while Theorem 4 leads to a less settling-like time.

B. Comparison Between PIO and Luenberger observer

In this subsection, simulations are conducted under different types of observers (i.e. PIO and Luenberger observer) to evaluate their respective estimation effect. Fig. 6 depicts the evolutions of the estimation error dynamics with PIO and Fig. 7 plots the evolutions of the estimation error dynamics with Luenberger observer. It is evident from Figs. 6-7 that the PIO outperforms the Luenberger observer in terms of the estimation performance.

C. Effect of Packet-Dropout Probabilities on Estimation Errors and Decoding errors

In this subsection, let us reveal the influence of packet dropouts on estimation performance and decoding accuracy. To accomplish this, we repeat the simulations 100 times and calculate the average value of minimum upper bound for estimation error and decoding error with different packet-dropout probabilities, and the corresponding results are shown in the Tables II-III. Intuitively, with the increase of packet loss rate (the decrease of $\bar{\phi}_u$ or $\bar{\phi}_d$), both the estimation performance and decoding accuracy deteriorate.

V. Conclusions

In this paper, the PIO design issue has been addressed for a class of ANNs in the presence of bounded disturbance. A

This article has been accepted for publication in a future issue of this journal, but has not been fully edited. Content may change prior to final publication.
Citation information: DOI: 10.1109/TNNLS.2022.3209632, IEEE Transactions on Neural Networks and Learning Systems

TABLE II: The minimum upper bounds of estimation error and decoding error subject to different $\bar{\phi}_u$ for $\bar{\phi}_d = 0.01$

$\bar{\phi}_u$	Minimum upper bounds of estimation error		Minimum upper bounds of decoding error
	Theorem 3	Theorem 4	
0.99	0.031	0.057	1.076
0.89	0.052	0.079	2.694
0.79	0.068	0.082	2.758
0.69	0.075	0.093	3.129
0.59	0.098	0.154	3.236
0.49	0.104	0.317	4.078
0.39	0.297	0.725	4.239
0.29	0.302	0.971	5.813
0.19	0.543	1.034	7.454
0.09	0.679	1.146	8.071

TABLE III: The minimum upper bounds of estimation error and decoding error subject to different $\bar{\phi}_u$ for $\bar{\phi}_d = 0.99$

$\bar{\phi}_u$	Minimum upper bounds of estimation error		Minimum upper bounds of decoding error
	Theorem 3	Theorem 4	
0.91	0.011	0.026	0.236
0.81	0.015	0.029	0.459
0.71	0.018	0.032	0.537
0.61	0.021	0.034	0.641
0.51	0.023	0.038	0.796
0.41	0.026	0.043	0.958
0.31	0.029	0.045	1.239
0.21	0.031	0.052	1.512
0.11	0.037	0.058	1.731
0.01	0.039	0.061	1.804

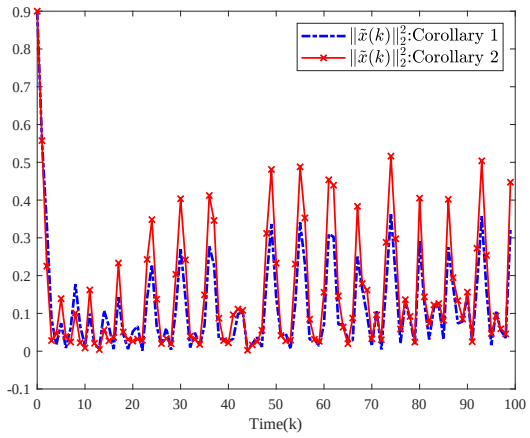

Fig. 7: Trajectories of $\|\tilde{x}(k)\|^2$ subject to *Corollary 1* and *Corollary 2*.

MDES has been employed to convert the measurement signal into corresponding codewords, aiming at further improving the reliability of the communication channel. The codewords transmissions (from the encoders to the decoders) have undergone random occurring packet dropouts whose random nature has been described by two sequences of Bernoulli-distributed random variables. Making good use of the stochastic analysis technique and the Lyapunov method, the effect of the packet dropouts on the decoding accuracy has been examined and the boundedness of estimation error dynamics has been analyzed. For the sake of guaranteeing two different estimation performance indices, two optimization problems have been resolved to obtain the PIO gains. Finally, a simulation example has been provided to evaluate the developed PIO design scheme. Our future research themes include the adoption of our main results to more complex systems, such as complex networks, multi-agent systems and wireless sensor networks [11], [23], [41], [44].

REFERENCES

[1] C. K. Ahn, P. Shi and L. Wu, Receding horizon stabilization and disturbance attenuation for neural networks with time-varying delay, *IEEE Transactions on Cybernetics*, vol. 45, no. 12, pp. 2680–2692, Dec. 2015.
[2] H. Bai, M. Zhang, A. Wang, M. Liu and Y. Zhao, Multiple description video coding using inter- and intra-description correlation at macro block level, *IEICE Transactions on Information and Systems*, vol. E97-D, no. 2, pp. 384–387, Feb. 2014.
[3] F. Bakhshande and D. Söffker, Proportional-integral-observer: A brief survey with special attention to the actual methods using acc benchmark, *IFAC-PapersOnLine*, vol. 48, no. 1, pp. 532–537, 2015.
[4] S. Beale and B. Shafai, Robust control system design with a proportional integral observer, *International Journal of Control*, vol. 50, no. 1, pp. 97–111, Apr. 1989.

[5] Y. Berrouche and R. E. Bekka, Improved multiple description wavelet based image coding using Hadamard transform, *AEU-International Journal of Electronics and Communications*, vol. 68, no. 10, pp. 976–982, Oct. 2014.

[6] J.-L. Chang, Applying discrete-time proportional integral observers for state and disturbance estimations, *IEEE Transactions on Automatic Control*, vol. 51, no. 5, pp. 814–818, May 2006.

[7] Y. Chen, J. Ren, X. Zhao and A. Xue, State estimation of Markov jump neural networks with random delays by redundant channels, *Neurocomputing*, vol. 453, pp. 493–501, Sept. 2021.

[8] Y. Chen, Q. Song, Z. Zhao, Y. Liu and F. E. Alsaadi, Global Mittag-Leffler stability for fractional-order quaternion-valued neural networks with piecewise constant arguments and impulses, *International Journal of Systems Science*, vol. 53, no. 8, pp. 1756–1768, Jun. 2022.

[9] P. Correia, P. A. Assuncao and V. Silva, Multiple description of coded video for path diversity streaming adaptation, *IEEE Transactions on Multimedia*, vol. 14, no. 3, pp. 923–935, Jun. 2012.

[10] S.-L. Dai, S. He, M. Wang and C. Yuan, Adaptive neural control of underactuated surface vessels with prescribed performance guarantees, *IEEE Transactions on Neural Networks and Learning Systems*, vol. 30, no. 12, pp. 3686–3698, Dec. 2019.

[11] S. Feng, H. Yu, C. Jia and P. Gao, Joint state and fault estimation for nonlinear complex networks with mixed time-delays and uncertain inner coupling: Non-fragile recursive method, *Systems Science & Control Engineering*, vol. 10, no. 1, pp. 603–615, Dec. 2022.

[12] M. Hernandez-Gonzalez, E. A. Hernandez-Vargas and M. V. Basin, Discrete-time high order neural network identifier trained with cubature Kalman filter, *Neurocomputing*, vol. 322, pp. 13–21, Dec. 2018.

[13] Z. Jin, V. Gupta and R. M. Murry, State estimation over packet dropping networks using multiple description coding, *Automatica*, vol. 42, no. 9, pp. 1441–1452, Sept. 2006.

[14] X. Kan, Y. Fan, Z. Fang, L. Cao, N. N. Xiong, D. Yang and X. Li, A novel IoT network intrusion detection approach based on Adaptive Particle Swarm Optimization Convolutional Neural Network, *Information Sciences*, vol. 568, pp. 147–162, Aug. 2021.

[15] D. Kapetanovic, S. Chatzinotas and B. Ottersten, Index assignment for multiple description repair in distributed storage systems, in *Proceedings of the 2014 IEEE International Conference on Communications*, pp. 3896–3901, Sydney, Australia, Jun. 10–14, 2014.

[16] L. Ke, Y. Zhang, B. Yang, Z. Luo and Z. Liu, Fault diagnosis with synchrosqueezing transform and optimized deep convolutional neural network: An application in modular multilevel converters, *Neurocomputing*, vol. 430, pp. 24–33, Mar. 2021.

[17] K.-S. Kim, K.-H. Rew and S. Kim, Disturbance observer for estimating higher order disturbances in time series expansion, *IEEE Transactions on Automatic Control*, vol. 55, no. 8, pp. 1905–1911, Aug. 2010.

[18] D. Koenig, Unknown input proportional multiple-integral observer design for linear descriptor systems: Application to state and fault estimation, *IEEE Transactions on Automatic Control*, vol. 50, no. 2, pp. 212–217, Feb. 2005.

[19] R. Kozma and M. Puljic, Hierarchical random cellular neural networks for system-level brain-like signal processing, *Neural Networks*, vol. 45, no. 9, pp. 101–110, Sept. 2013.

[20] J. Li, H. Dong, Z. Wang and X. Bu, Partial-neurons-based passivity-guaranteed state estimation for neural networks with randomly occurring time delays, *IEEE Transactions on Neural Networks and Learning Systems*, vol. 31, no. 9, pp. 3747–3753, Sept. 2020.

[21] Q. Li, J. Liang and H. Qu, H_∞ estimation for stochastic semi-Markovian switching CVNNs with missing measurements and mode-dependent delays, *Neural Networks*, vol. 141, pp. 281–293, Sept. 2021.

[22] Y. Liu, B. Shen and H. Shu, Finite-time resilient H_∞ state estimation for discrete-time delayed neural networks under dynamic event-triggered mechanism, *Neural Networks*, vol. 121, pp. 356–365, Jan. 2020.

[23] Y. Shi, L. Yao and S. Li, Adaptive synchronization control for stochastic complex networks with derivative coupling, *Systems Science & Control Engineering*, vol. 10, no. 1, pp. 698–709, Dec. 2022.

[24] Y. Liu, Z. Wang, Y. Yuan and W. Liu, Event-triggered partial-nodes-based state estimation for delayed complex networks with bounded distributed delays, *IEEE Transactions on Systems, Man, and Cybernetics - Systems*, vol. 49, no. 6, pp. 1088–1098, Jun. 2019.

[25] R. Lu, P. Shi, H. Su, Z.-G. Wu and J. Lu, Synchronization of general chaotic neural networks with nonuniform sampling and packet missing: A switched system approach, *IEEE Transactions on Neural Networks and Learning Systems*, vol. 29, no. 3, pp. 523–533, Mar. 2018.

[26] X. Nie, J. Liang and J. Cao, Multistability analysis of competitive neural networks with Gaussian-wavelet-type activation functions and unbounded time-varying delays, *Applied Mathematics and Computation*, vol. 356, pp. 449–468, Sept. 2019.

[27] H. H. Niemann, J. Stoustrup, B. Shafai and S. Beale, LTR design of proportional-integral observers, *International Journal of Robust and Nonlinear Control*, vol. 5, no. 7, pp. 671–693, 1995.

[28] W. Qian, Y. Li, Y. Zhao and Y. Chen, New optimal method for L_2-L_∞ state estimation of delayed neural networks, *Neurocomputing*, vol. 415, pp. 258–265, Nov. 2020.

[29] H. Qiao, J. Peng and Z.-B. Xu, Nonlinear measures: A new approach to exponential stability analysis for Hopfield-type neural networks, *IEEE Transactions on Neural Networks*, vol. 12, no. 2, pp. 360–370, Mar. 2001.

[30] M. A. Rana, F. Ndiaye, S. A. Chowdhury and N. Mansoor, Multiple description image transmission for diversity systems over unreliable communication networks, in *Proceedings of 10th International Conference on Computer and Information Technology*, pp. 240–244, Dhanmondi, Bangladesh, Dec. 27–29, 2007.

[31] B. Shafai, S. Beale, H. H. Niemann and J. L. Stoustrup, LTR design of discrete-time proportional-integral observers, *IEEE Transactions on Automatic Control*, vol. 41, no. 7, pp. 1056–1062, Jul. 1996.

[32] D. Söffker, T. J. Yu and P. C. Müller, State estimation of dynamical systems with nonlinearities by using proportional-integral observer, *International Journal of Systems Science*, vol. 26, no. 9, pp. 1571–1582, Nov. 1995.

[33] Q. Song, Y. Chen, Z. Zhao, Y. Liu and F. E. Alsaadi, Robust stability of fractional-order quaternion-valued neural networks with neutral delays and parameter uncertainties, *Neurocomputing*, vol. 420, pp. 70–81, Jan. 2021.

[34] J. Suo, N. Li and Q. Li, Event-triggered H_∞ state estimation for discrete-time delayed switched stochastic neural networks with persistent dwell-time switching regularities and sensor saturations, *Neurocomputing*, vol. 455, pp. 297–307, Sept. 2021.

[35] H. Tao, H. Tan, Q. Chen, H. Liu and J. Hu, H_∞ state estimation for memristive neural networks with randomly occurring DoS attacks, *Systems Science & Control Engineering*, vol. 10, no. 1, pp. 154–165, Dec. 2022.

[36] V. A. Vaishampayan, Design of multiple description scalar quantizers, *IEEE Transactions on Information Theory*, vol. 39, no. 3, pp. 821–834, May 1993.

[37] L. Wang, S. Liu, Y. Zhang, D. Ding and X. Yi, Non-fragile l_2-l_∞ state estimation for time-delayed artificial neural networks: An adaptive event-triggered approach, *International Journal of Systems Science*, vol. 53, no. 10, pp. 2247–2259, Jul. 2022.

[38] L. Wang, Z. Wang, G. Wei and F. E. Alsaadi, Finite-time state estimation for recurrent delayed neural networks with component-based event-triggering protocol, *IEEE Transactions on Neural Networks and Learning Systems*, vol. 29, no. 4, pp. 1046–1057, Apr. 2018.

[39] P. Wen, X. Li, N. Hou and S. Mu, Distributed recursive fault estimation with binary encoding schemes over sensor networks, *Systems Science & Control Engineering*, vol. 10, no. 1, pp. 416–426, Dec. 2022.

[40] F. Yang, J. Li, H. Dong and Y. Shen, Proportional-integral-type estimator design for delayed recurrent neural networks under encoding-decoding mechanism, *International Journal of Systems Science*, in press, DOI: 10.1080/00207721.2022.2063968.

[41] Z. Yang, Y. Liu, W. Zhang, F. E. Alsaadi and K. H. Alharbi, Differentially private containment control for multi-agent systems, *International Journal of Systems Science*, in press, DOI: 10.1080/00207721.2022.2070794.

[42] J. Yang, L. Ma, Y. Chen and X. Yi, L_2-L_∞ state estimation for continuous stochastic delayed neural networks via memory event-triggering strategy, *International Journal of Systems Science*, in press, DOI: 10.1080/00207721.2022.2055192.

[43] Y. Xu, R. Lu, P. Shi, J. Tao and S. Xie, Robust estimation for neural networks with randomly occurring distributed delays and Markovian jump coupling, *IEEE Transactions on Neural Networks and Learning Systems*, vol. 29, no. 4, pp. 845–855, Apr. 2018.

[44] L. Yu, Y. Cui, Y. Liu, N. D. Alotaibi and F. E. Alsaadi, Sampled-based consensus of multi-agent systems with bounded distributed time-delays and dynamic quantisation effects, *International Journal of Systems Science*, vol. 53, no. 11, pp. 2390–2406, Aug. 2022.

[45] D. Zhang, Q.-L. Han and X.-M. Zhang, Network-based modeling and proportional-integral control for direct-drive-wheel systems in wireless network environments, *IEEE Transactions on Cybernetics*, vol. 50, no. 6, pp. 2462–2474, Jun. 2020.

[46] D. Zhao, Z. Wang, G. Wei and Y. Chen, Proportional-integral observer design for multi-delayed sensor-saturated recurrent neural networks: A dynamic event-triggered protocol, *IEEE Transactions on Cybernetics*, vol. 50, no. 11, pp. 4619–4632, Nov. 2020.

[47] D. Zhao, Z. Wang, G. Wei and X. Liu, Non-fragile H_∞ state estimation for recurrent neural networks with time-varying delays: On proportional-integral observer design, *IEEE Transactions on Neural*

Networks and Learning Systems, vol. 32, no. 8, pp. 3553—3565, Aug. 2021.

[48] Z. Zuo, C. Yang and Y. Wang, A new method for stability analysis of recurrent neural networks with interval time-varying delay, *IEEE Transactions on Neural Networks*, vol. 21, no. 2, pp. 339–344, Feb. 2010.

Di Zhao received the B.Sc. degree in Mathematics from Jilin Normal University, Siping, China, in 2013 and the Ph.D. degree in Control Science and Engineering from University of Shanghai for Science and Technology, Shanghai, China, in 2020. She is currently a Postdoctoral Research Fellow with the College of Science, University of Shanghai for Science and Technology, Shanghai, China.

From November 2018 to November 2019, she was a visiting Ph.D. student in the Department of Computer Science, Brunel University London, Uxbridge, U.K.. From March to June 2018, she was a Research Associate in the Department of Mathematics, City University of Hong Kong, Hong Kong.

Dr. Zhao's research interests include PID control, proportional-integral observer, networked control systems and cyber-physical systems. She is currently a reviewer for some international journals.

Zidong Wang (Fellow, IEEE) was born in Jiangsu, China, in 1966. He received the B.Sc. degree in mathematics in 1986 from Suzhou University, Suzhou, China, and the M.Sc. degree in applied mathematics in 1990 and the Ph.D. degree in electrical engineering in 1994, both from Nanjing University of Science and Technology, Nanjing, China.

He is currently Professor of Dynamical Systems and Computing in the Department of Computer Science, Brunel University London, U.K. From 1990 to 2002, he held teaching and research appointments in universities in China, Germany and the UK. Prof. Wang's research interests include dynamical systems, signal processing, bioinformatics, control theory and applications. He has published more than 700 papers in international journals. He is a holder of the Alexander von Humboldt Research Fellowship of Germany, the JSPS Research Fellowship of Japan, William Mong Visiting Research Fellowship of Hong Kong.

Prof. Wang serves (or has served) as the Editor-in-Chief for *International Journal of Systems Science*, the Editor-in-Chief for *Neurocomputing*, the Editor-in-Chief for *Systems Science & Control Engineering*, and an Associate Editor for 12 international journals including IEEE Transactions on Automatic Control, IEEE Transactions on Control Systems Technology, IEEE Transactions on Neural Networks, IEEE Transactions on Signal Processing, and IEEE Transactions on Systems, Man, and Cybernetics-Part C. He is a Member of the Academia Europaea, a Member of the European Academy of Sciences and Arts, an Academician of the International Academy for Systems and Cybernetic Sciences, a Fellow of the IEEE, a Fellow of the Royal Statistical Society and a member of program committee for many international conferences.

Yun Chen was born in Zhejiang Province, China, in 1976. He received the B.E. degree in thermal engineering in 1999 from Central South University of Technology (Central South University), China, and the M.E. degree in engineering thermal physics in 2002 and Ph.D. degree in control science and engineering in 2008, both from Zhejiang University, China. He is currently a Professor in Hangzhou Dianzi University, China.

Guoliang Wei received the B.Sc. degree in mathematics from Henan Normal University, Xinxiang, China, in 1997, and the M.Sc. degree in applied mathematics and the Ph.D. degree in control engineering from Donghua University, Shanghai, China, in 2005 and 2008, respectively.

He is currently a Professor with the Business School, University of Shanghai for Science and Technology, Shanghai, China. From March 2010 to May 2011, he was an Alexander von Humboldt Research Fellow with the Institute for Automatic Control and Complex Systems, University of Duisburg-Essen, Duisburg, Germany. From March 2009 to February 2010, he was a Postdoctoral Research Fellow with the Department of Information Systems and Computing, Brunel University, Uxbridge, U.K., sponsored by the Leverhulme Trust of the U.K. From June 2007 to August 2007, he was a Research Assistant with the University of Hong Kong, Hong Kong. From March 2008 to May 2008, he was a Research Assistant with the City University of Hong Kong, Hong Kong. He has published more than 100 papers in refereed international journals. His research interests include nonlinear systems, stochastic systems, and bioinformatics.

Prof. Wei is a very active reviewer for many international journals.

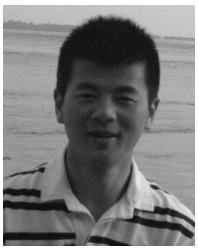

Weiguo Sheng received the M.Sc. degree in information technology from the University of Nottingham, U.K., in 2002 and the Ph.D. degree in computer science from Brunel University, U.K., in 2005. Then, he worked as a Researcher at the University of Kent, U.K. and Royal Holloway, University of London, U.K. He is currently a Professor at Hangzhou Normal University. His research interests include evolutionary computation, data mining/clustering, pattern recognition and machine learning.